Zircon geochemistry records the action of metamorphic fluid on the formation of ultrahigh-pressure jadeite quartzite...

Article *in* Chemical Geology · November 2015

DOI: 10.1016/j.chemgeo.2015.10.043

5 authors, including:

Xiao-Ying Gao
University of Science and Technology of China

Yong-Fei Zheng
University of Science and Technology of China

Yi-Xiang Chen
University of Science and Technology of China

Wancai Li
University of Science and Technology of China

Chemical Geology 419 (2015) 158–175

Contents lists available at ScienceDirect

Chemical Geology

journal homepage: www.elsevier.com/locate/chemgeo

Zircon geochemistry records the action of metamorphic fluid on the formation of ultrahigh-pressure jadeite quartzite in the Dabie orogen

Xiao-Ying Gao [a,*], Yong-Fei Zheng [a], Yi-Xiang Chen [a], Hao-Lan Tang [b], Wan-Cai Li [a]

[a] CAS Key Laboratory of Crust-Mantle Materials and Environments, School of Earth and Space Sciences, University of Science and Technology of China, Hefei 230026, China
[b] Department of Earth and Space Science, University of California, Los Angeles, CA 90095, USA

ARTICLE INFO

Article history:
Received 11 March 2015
Received in revised form 20 October 2015
Accepted 30 October 2015
Available online 31 October 2015

Keywords:
Jadeite quartzite
Subduction zone
Protolith zircon
Fluid metasomatism
UHP metamorphism

ABSTRACT

A combined study of mineral inclusions, U–Pb ages, trace elements and Hf-O isotopes was carried out for zircons from a coesite-bearing jadeite quartzite in the Dabie orogen. The results provide insights into the action of ultrahigh-pressure (UHP) metamorphic fluids during continental deep subduction to a mantle depth and thus constraints on the origin of the jadeite quartzite in the continental subduction zone. The zircons mostly show core-rim structures in cathodoluminescence images. The overgrown rims contain rare mineral inclusions, and exhibit concordant U–Pb ages of 225 to 246 Ma and flat HREE patterns with negligible Eu anomalies. In contrast, the relict cores contain UHP metamorphic mineral inclusions such as coesite, jadeite and rutile, and show discordant U–Pb ages ranging from 983 to 2045 Ma and steep REE patterns with significant negative Eu anomalies. The U–Pb isotope data for the all cores and rims define an apparent discordia line with upper and lower intercept ages of 2000 ± 43 Ma and 234 ± 18 Ma, respectively. We interpret the rims with Triassic ages as the new growth of metamorphic origin and the cores with Precambrian ages as the protolith relics of magmatic origin. The relict magmatic zircons underwent two subtypes of metamorphic recrystallization, i.e., solid-state transformation and metasomatic alteration. The solid-state recrystallized zircons exhibit slightly discordant U–Pb ages close to the protolith age, steep MREE–HREE patterns, and almost unchanged Hf isotope ratios. These observations point to the lowest degree of resetting to the geochemical composition of protolith zircons. In contrast, the metasomatically recrystallized zircons exhibit partial resetting in protolith zircon REE composition and U–Pb and Lu–Hf isotopic systems. All of the zircon domains, regardless of the rims and cores, show relatively consistent $\delta^{18}O$ values of 4.0 ± 0.2‰. Such a consistency indicates not only that the metamorphic fluids are of internal origin from the deeply subducted continental crust but also that the oxygen isotope composition of protolith zircons was reequilibrated with the UHP metamorphic fluids of Triassic age. The metasomatic recrystallization of protolith zircons is indicated by the occurrence of UHP inclusion minerals such as coesite, rutile and jadeite in sealed microcracks. In this regard, the fluid metasomatism firstly took place along fractures of the relict zircons during prograde subduction of the continental crust and then experienced the metamorphic recrystallization to result in sealing of the fractures under the UHP conditions. As such, the metasomatic recrystallization has heterogeneously reset the U–Pb and Lu–Hf isotope systems of protolith zircons. The composition of inclusion minerals within the relict zircon cores suggests that the metamorphic fluids were rich in Si, Ti, Na and Al. These elements would be acquired by the metamorphic fluids through metasomatic reaction of metagreywackes overlying the granitic orthogneiss. Therefore, the jadeite quartzite would be precipitated from the UHP metamorphic fluids that were derived from dehydration of the underlying basement orthogneiss but reacted with the metagreywackes during the continental subduction-zone metamorphism.

1. Introduction

Jadeitites and jadeite-rich lithologies are relatively rare rocks on Earth. They are composed predominantly of jadeite and typically associated with tectonic blocks of high-pressure (HP) to ultrahigh-pressure (UHP) metabasites (e.g., eclogites, blueschists) in oceanic and continental subduction zones (Schertl et al., 2012; Tsujimori and Harlow, 2012; Harlow et al., 2015). In general, most jadeitites and jadeite-bearing rocks are interpreted as precipitating directly from metamorphic fluids, or metasomatic replacement of a protolith via metamorphic fluids (Shi et al., 2005; Harlow et al., 2007, 2015; Yui et al., 2010; Tsujimori and Harlow, 2012; Schertl et al., 2012; Yui and Fukuyama, 2015). In either case, the metamorphic fluids are required to dissolve Na, Al and Si from host rocks through extensive infiltration and fluid-mineral reaction for the eventual formation of jadeitite and jadeite-rich rocks. Jadeite may form through the decomposition of albite during prograde metamorphism (e.g., Holland, 1980; Zhai et al., 1992; Liou et al., 1997; Su

* Corresponding author.
E-mail address: gaoying@ustc.edu.cn (X.-Y. Gao).

http://dx.doi.org/10.1016/j.chemgeo.2015.10.043
0009-2541/

et al., 1996, 2004; Zhang et al., 2014). It may also decompose to albite and nepheline when the temperature decreases at a certain pressure (Gasparik, 1990; Prewitt and Burnham, 1996).

Jadeite quartzite is basically a two-phase rock that is mainly composed of jadeite and quartz. It is also a rare rock type in continental subduction zones where it commonly occurs as intercalations in pyrope quartzites (e.g., Chopin, 1984; Schertl and Schreyer, 2008), mafic eclogites (e.g., Dobretsov, 1963; Sobolev et al., 1986; Bröcker and Keasling, 2006; Schertl et al., 2012) and felsic gneisses (e.g., Zhai et al., 1992; Okay, 1993; Zhang et al., 1995; Liou et al., 1997). Although many studies of petrology, geochemistry, geochronology and microfabrics have been devoted to jadeite quartzite, it still remains to answer the following questions. What is the protolith of jadeite quartzite? How did jadeite quartzite form during subduction-zone metamorphism? Why did jadeite quartzite form in different subduction zones? If jadeite quartzite would also form through a metasomatic process like jadeitite and jadeite-rich rocks, a resolution to its origin will provide insights into the nature of metamorphic fluids attending the fluid–rock interaction in continental subduction zones.

Accessory minerals such as zircon, rutile and titanite widely occur in UHP metamorphic rocks, especially in jadeite quartzite (e.g., Wang et al., 1995, 2010; Cong et al., 1995; Liou et al., 1997). These accessory minerals usually exhibit complex responses to fluid action during subduction-zone metamorphism (Rubatto and Hermann, 2003; Su et al., 2004; Zheng et al., 2007; Gregory et al., 2009; Gao et al., 2011; W.-C. Li et al., 2013). Among them zircon has been a very important one because it can serve as a sensitive monitor of fluid-rock interaction during subduction-zone processes (e.g., Zheng, 2009; Fu et al., 2010; Hermann et al., 2013). As a refractory mineral, protolith zircon is resistant to metamorphic reaction and thus essentially inert in the absence of metamorphic fluids. As soon as the metamorphic fluids are accessible, however, the protolith zircon may experience variable degrees of recrystallization via the mechanisms of solid-state transformation, dissolution reprecipitation, and metasomatic alteration along fractures and crystal boundaries (Hoskin and Black, 2000; Hoskin and Schaltegger, 2003; Xia et al., 2009, 2010, 2013; Chen et al., 2010, 2011; Liu et al., 2012). On the other hand, zircon may newly grow by metamorphic reactions of protolith minerals under subsolidus conditions (e.g., Fraser et al., 1997; Rubatto, 2002), or precipitated from aqueous fluids (e.g., Rubatto and Hermann, 2003; Zheng et al., 2007; Chen et al., 2010) or hydrous melts (e.g., Xia et al., 2009; Chen et al., 2013a, 2013b; W.-C. Li et al., 2013). In either case, the property of metamorphic fluids is a key not only to the recrystallization of protolith zircons under subduction-zone conditions (e.g., Rubatto and Hermann, 2007; Xia et al., 2009, 2010, 2013; Chen et al., 2010, 2011; Liu et al., 2012; Li et al., 2014) but also the growth of metamorphic and anatectic zircons (Zheng et al., 2007; Zheng, 2009; Chen et al., 2012; W.-C. Li et al., 2013; Li et al., 2014).

Both metamorphosed and metamorphic zircons occur in many UHP metamorphic rocks (e.g., Zheng, 2009; Liu and Liou, 2011; Hermann et al., 2013). The protolith zircon may suffer variable extents of modification via the different mechanisms of recrystallization during subduction-zone metamorphism, mainly depending on zircon crystallinity and fluid accessibility (Xia et al., 2009, 2010; Chen et al., 2010, 2011). Generally, the modification is not significant at low metamorphic grades where non-metamict protolith zircons tend to survive, although they can be mechanically fractured (Wayne and Sinha, 1992; Hoskin and Schaltegger, 2003). At higher metamorphic grades, the protolith zircon may be significantly altered by metamorphic fluids to result in partial to complete resetting of geochemical compositions (e.g., Martin et al., 2008; Xia et al., 2009, 2010; Chen et al., 2010, 2011, 2012, 2013a, 2013b). The redistribution of geochemical compositions may be recorded by compositional variations of metamorphosed zircons during HP to UHP metamorphism (Möller et al., 2003; Xia et al., 2009, 2013; Chen et al., 2010, 2011). The great advantage of zircon as a fluid monitor is that it can be accurately dated by the U–Pb method, providing an absolute age for fluid action (Zheng, 2009; Chen et al., 2012; Hermann et al., 2013). Either metamorphic or metamorphosed zircons can be used to trace the fluid-rock interaction during subduction-zone processes (Chen et al., 2010; Zheng, 2012; Xia et al., 2013). Therefore, the fluid action during subduction-zone metamorphism can be deduced from various records of zircons in HP to UHP metamorphic rocks (Zheng, 2009; Hermann et al., 2013).

The role of metamorphic fluids during the recrystallization of protolith zircon by dissolution-reprecipitation and subsequent compositional changes has been evaluated by several studies (e.g., Geisler et al., 2001; Hoskin and Schaltegger, 2003; Xia et al., 2010). Upon the fluid action, the protolith zircon is susceptible to reworking along grain surface and internal fractures due to fluid infiltration and exchange (e.g., Valley et al., 1994; Xia et al., 2013). The precipitation of jadeite from metamorphic fluids indicates their alkalic property, which has a capacity to dissolve some fluid-immobile incompatible trace elements such as Zr (e.g., Zheng et al., 2007). The occurrence of zircons in jadeite quartzites provides us with an excellent opportunity to decipher the action of metamorphic fluids on the modification of protolith zircons. The U–Pb dating and geochemical analysis of metamorphic and metamorphosed zircons from UHP metamorphic rocks can provide insights into the action of deep fluids during subduction-zone processes (e.g., Rubatto and Hermann, 2007; Xia et al., 2009, 2010; Chen et al., 2010, 2012; Hermann et al., 2013). Thus, an integrated study of mineral inclusions, U–Pb ages and geochemical compositions in zircon from jadeite quartzites can provide constraints not only on the property and time of fluid action, but also on the mobility of elements and isotopes in subduction zones.

In order to decipher the action of metamorphic fluids in the petrogenesis of jadeite quartzites, we have carried out a combined study of zircon U–Pb ages, trace elements, and Lu–Hf and O isotopes, together with microscopic observation, cathodoluminescence (CL) imaging and laser Raman analysis, for UHP jadeite quartzite from the Dabie orogen in China. The results provide new insights not only into the origin of different zircon domains but also into the time and conditions of fluid action during continental subduction-zone metamorphism. A further constraint on the protolith nature of jadeite quartzite is also provided by the present study.

2. Geological setting and sample

The Dabie orogen is located between the South China Block and North China Block in east-central China (insert in Fig. 1a). It belongs to the western segment of the Dabie-Sulu orogenic belt, which was separated by the Tanlu Fault into western and eastern segments, named as the Dabie and Sulu orogens, respectively. The Dabie-Sulu orogenic belt was built by the Triassic subduction of the South China Block beneath the North China Block (e.g., Wang et al., 1995; Li et al., 1999; Zheng et al., 2009). The findings of coesite (Okay et al., 1989; Wang et al., 1989) and microdiamond (Xu et al., 1992) inclusions in metamorphic minerals from the Dabie-Sulu orogenic belt have provided petrological evidence for the deep subduction of continental crust to mantle depths of >100 km. The Dabie orogen is composed of several fault-bounded metamorphic units. Based on the lithotectonic characteristics (Zheng et al., 2005; Zheng, 2008), it is subdivided into five major zones from north to south (Fig. 1a): (1) the Beihuaiyang low-T/low-P greenschist-facies zone; (2) the North Dabie high-T/UHP granulite-facies zone with migmatization; (3) the Central Dabie mid-T/UHP eclogite-facies zone; (4) the South Dabie low-T/UHP eclogite-facies zone; (5) the Susong low-T/HP blueschist-facies zone. The metamorphic grade increases from south to north, except the Beihuaiyang zone that is the accretionary wedge formed at the early stage of continental subduciton (Zheng et al., 2005). Jurassic–Cretaceous sedimentary rocks occur in the southern margin of the North China Block.

Mafic eclogites mainly occur in the mid-T/UHP eclogite-facie zone in the Dabie orogenic belt, with granitic gneisses as the major host for them. Three major metamorphic stages can be retrieved for the mid-

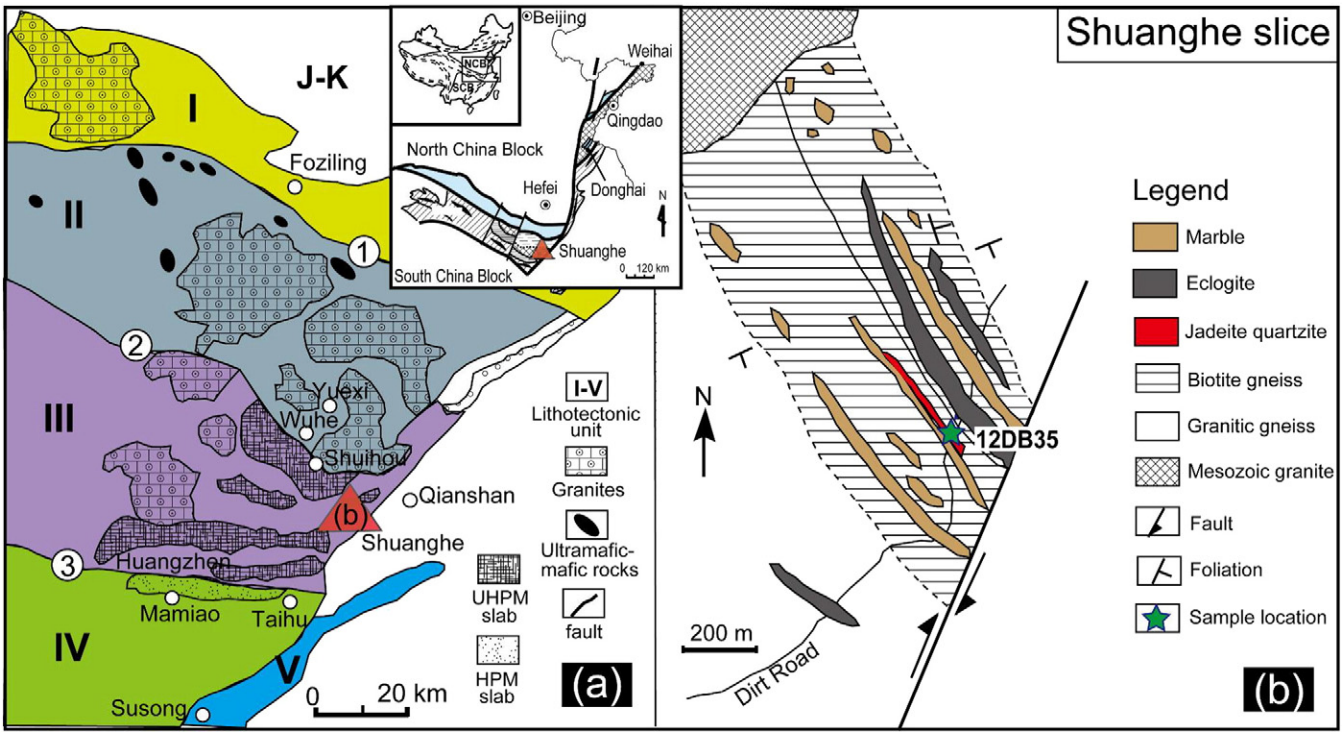

Fig. 1. Sketch map of geology in the Dabie orogen and the UHP metamorphic slice at Shuanghe in Central Dabie (revised after Zheng et al., 2003). (a) The Dabie orogen, in which insert denotes the position of the Dabie-Sulu orogenic belt in east-central China; (b) the UHP metamorphic slice at Shuanghe in the Central Dabie mid-T/UHP eclogite-facies zone. Lithotectonic units in the Dabie orogen: (I) the Beihuaiyang low-T/low-P greenschist-facies zone; (II) the North Dabie high-T/UHP granulite-facies zone; (III) the Central Dabie mid-T/UHP eclogite-facies zone; (IV) the South Dabie low-T/UHP eclogite-facies zone; and (V) the Susong low-T/HP blueschist-facies zone. Circled number denotes the faults: ① Xiaotian-Mozitan Fault, ② Wuhe-Shuihou Fault, and ③ Mamiao-Taihu Fault. J-K denotes the sedimentary sequence of Jurassic to Cretaceous in the southern margin of the North China Block.

T/UHP metamorphic rocks in this zone (Cong et al., 1995; Gao et al., 2011; Liou et al., 2009; Zheng et al., 2003, 2011): (1) peak UHP coesite/diamond eclogite-facies, with metamorphic temperatures of 700–750 °C and pressures of >2.8 GPa; (2) HP quartz eclogite-facies retrograde recrystallization, with P–T conditions from 850 to 750 °C at 2.5–2.0 GPa to 650–600 °C at 2.0–1.0 GPa; (3) amphibolite-facies retrogression, with P–T conditions of 600–450 °C and 1.0–0.6 GPa. Generally, the granitic orthogneisses are a poor recorder of UHP metamorphism because felsic UHP metamorphic parageneses are susceptible to retrogression and thus frequently reequilibrated at amphibolite-facies conditions due to the action of retrograde fluids during exhumation (e.g., Chen et al., 2011; Liu and Liou, 2011; Tsai and Liou, 2000; Xiao et al., 2001; Zhang et al., 1995; Zheng et al., 2003).

This study deals with jadeite quartzite at Shuanghe in the eastern part of the Dabie orogen, which belongs to the mid-T/UHP eclogite-facies zone (Fig. 1b). Previous studies have examined the petrology, mineralogy, geochemistry and geochronology of UHP metamorphic rocks in this locality (e.g., Cong et al., 1995; Liou et al., 1997; Wu et al., 1998; Zheng et al., 1998; Li et al., 2000; Fu et al., 2001; Ayers et al., 2002; Gao et al., 2011). Petrological studies indicated that the peak metamorphic pressure for the UHP metamorphic rocks is greater than 2.8–3.3 GPa and the maximum temperature of 800–850 °C was reached

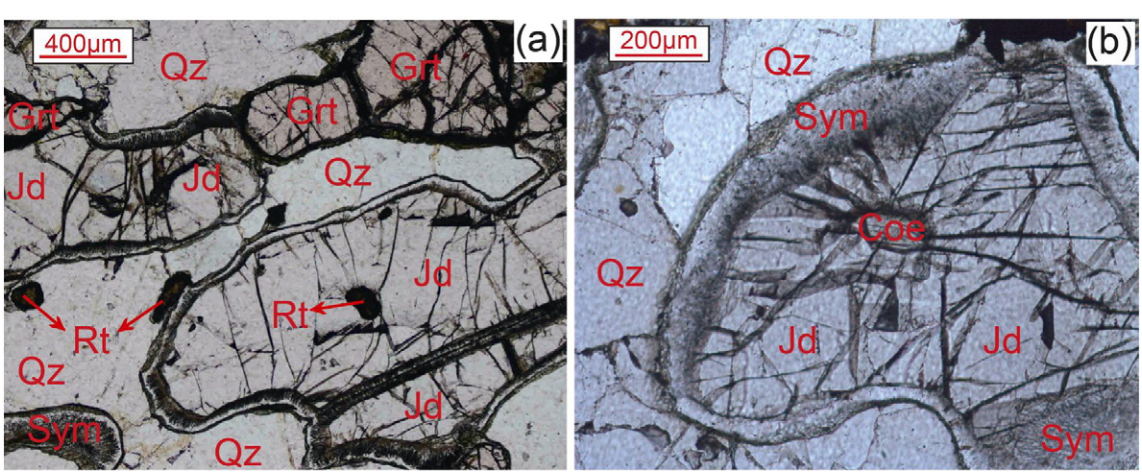

Fig. 2. Photomicrographs showing the texture and mineral paragenesis of jadeite quartzite from Shuanghe in the Dabie orogen (plane-polarized light, PPL). (a) Jadeite quartzite composed of quartz, jadeite and garnet with minor rutile and retrograde metamorphic minerals. The jadeite and garnet grains are partially replaced by symplectic mineral coronas; (b) coesite inclusion in jadeite with radial cracks.

during the exhumation of UHP metamorphic rocks (Okay, 1993; Cong et al., 1995; Carswell et al., 1997; Gao et al., 2011).

The jadeite quartzite used in this study occurs as lenses in the UHP granitic orthogneiss, with a weak deformation (Fig. 2). A sample (12DB35) has been investigated comprehensively. It is composed of jadeite (45–55%), quartz (35–45%), garnet (5%) and minor titanite, coesite, rutile, zircon and apatite. Previous studies indicated that the P–T path is similar for jadeite quartzite and the adjacent coesite-bearing eclogites and other UHP rocks in the Dabie orogen (Liou et al., 1997; Ayers et al., 2002; Liu et al., 2006). Jadeite and garnet grains are partially altered to form a corona texture (Fig. 2). Jadeite is composed of three zones based on altered mineral aggregates: (1) the inner zone that is composed of a fine fibrous symplectite of albite, taramite and preiswerkite; (2) the middle zone that has a coarse-grained plagioclase and amphibole corona; (3) the outer zone that is composed of a thin rim of green aegirine. Most garnet grains are rimmed by retrograde coronas composed of sodic amphibole and plagioclase. Relict coesite and its pseudomorphs occur in jadeite with well-developed radial fractures (Fig. 2), indicating that the jadeite quartzite experienced the UHP metamorphism. The occurrence of coesite is confirmed by the laser Raman analysis (Fig. 3).

3. Analytical methods

3.1. Whole-rock major and trace elements

Whole-rock powdered samples were prepared in an agate mortar for analysis. Major elements and trace elements were analyzed at ALS Chemex Company (Guangzhou, China), using an X-ray fluo-rescence spectrometer (XRF) and solution ICP-MS respectively. The analytical precision is better than ±2–5% for major elements and ±10% for most trace elements.

3.2. Mineral major elements

Major elements in rock-forming minerals were analyzed by a JEOL JXA-8100 electronic microprobe (EMP) at the State Key Laboratory of Geological Processes and Mineral Resources in China University of Geosciences (CUG), Wuhan. The acceleration voltage was set as 15 kV at a current of 20 nA. The beam diameter was normally set as 5 μm for all the minerals. Natural silicate standards were used, and raw data were reduced using conventional ZAF correction procedures. Mineral abbreviations are after Whitney and Evans (2010).

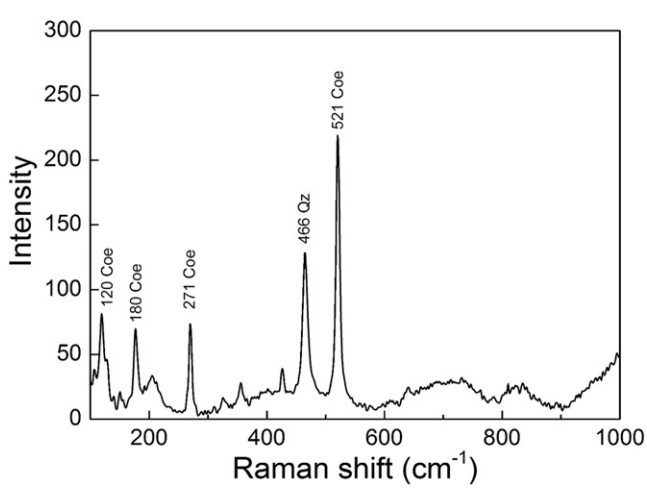

Fig. 3. Laser Raman spectra for coesite inclusion in jadeite from jadeite quartzite at Shuanghe in the Dabie orogen.

3.3. Mineral inclusions in zircon

Zircon separates were extracted by crushing, sieving and heavy liquid methods, and then purified by hand picking under a binocular microscope. Transparent zircon grains with few cracks were selected for U–Pb dating, and trace element and Lu–Hf isotope analyses. Zircon grains were mounted in epoxy resin and then polished down to expose the grain centre. The CL images and backscatter electronic (BSE) imaging of zircons were obtained on an FEI Sirion 200 Scanning electron microscope (SEM) at CAS Key Laboratory of Crust-Mantle Materials and Environments in University of Science and Technology of China (USTC), Hefei. The work conditions were at 20 kV and 15 nA during the CL imaging and at 20 kV and 18 nA during the BSE imaging. The CL images and optical photomicrographs were used to guide the analyses of mineral inclusions, U–Pb, Lu–Hf and O isotopes.

Element mapping for individual mineral inclusions within zircon was made on an energy dispersive spectrometry (EDS) Oxford Inca X-Max 50 equipped with a scanning electron microscope (SEM) (FEI Sirion 200) at CAS Key Laboratory of Crust-Mantle Materials and Environments in USTC, Hefei. The results were used to delineate the major element zoning and modal contents of mineral phases in the mineral inclusions. The measurements were carried out with an accelerating voltage of 20 kV, a spot size of ~2 μm and working distance of 15 mm.

Laser Raman analysis was undertaken by a Nicolet FT-Raman 960-ESP spectrometer with a 532 nm Ar laser excitation at room temperature at CAS Key Laboratory of Crust-Mantle Materials and Environments in USTC, Hefei. The beam size for Raman spectroscopy was ~1 μm. The Raman spectroscopy was used to identify the mineral inclusions of zircon in collaboration of optical observations. In order to check the precision and accuracy of the Raman data, the polystyrene and monocrystalline silicon were analyzed prior to and after the sample analytical session.

3.4. Zircon U–Pb ages and trace elements

In-situ analyses of zircon trace elements and U–Pb isotopes in the mounted zircon grains were simultaneously carried out by laser ablation-inductively coupling plasma mass spectrometer (LA-ICPMS) at State Key Laboratory of Geological Processes and Mineral Resources in China University of Geosciences, Wuhan. An Agilent 7500a Q-ICPMS was connected to a GeoLas-2005 193 nm excimer ArF laser-ablation system. The Agilent 7500a ICP-MS instrument was used to acquire ion-signal intensities. The Agilent ChemStation was utilized for the acquisition of each individual analysis. Based on a series of experiments, ablation spots were set to be 32 μm in this work, with 5 Hz repetition rate and laser energy of ~60 mJ. Each analysis incorporates a background acquisition interval of ~20 s before the laser is turned on. The laser ablation time is 40 s and the total acquisition time for an analysis is 100 s. The detailed analytical protocols and data reduction method have been presented by Liu et al. (2008, 2010).

Off-line selection, integration of background and analyte signals, time-drift correction and quantitative calibration for trace element analyses and U–Pb dating of zircon were performed by EXCEL software ICPMSDataCal (Liu et al., 2008, 2010). During the time-resolved analysis, contamination resulting from inclusions and fractures was monitored by index elements and only the relevant part of the signal was integrated. The zircon standard 91500 was used as an external standard to calibrate isotope fractionation. Preferred U–Pb isotope ratios used for zircon 91500 are from Wiedenbeck et al. (1995). Uncertainty of preferred values for the external standard 91500 was propagated to the ultimate results of samples. Zircon standard GJ-1 was analyzed as unknown sample. The obtained mean $^{206}Pb/^{238}U$ age for GJ-1 in this study is 603 ± 2 Ma (MSWD = 0.42, n = 21), consistent with the recommended value of 599.8 ± 1.7 Ma (Jackson et al., 2004). The common Pb correction was performed by the EXCEL program of ComPbCorr#3_151 (Andersen, 2002), assuming that the observed $^{206}Pb/^{238}U$, $^{207}Pb/^{235}U$ and $^{208}Pb/^{232}Th$ ratios for a discordant zircon can be accounted for by a

combination of lead loss at a defined time. Uncertainties of individual analyses are reported with 1σ errors; weighted-mean ages were calculated at 95% confidence level. Trace element concentrations were calibrated using ^{91}Zr as an internal reference and NIST SRM 610 as an external standard (Liu et al., 2010). The precision and accuracy of the analyses are better than ±10% (2σ) for most trace elements based on the replicate analyses of the reference material (GJ-1).

3.5. Zircon Lu–Hf isotopes

The LA-MC-ICPMS *in situ* Lu–Hf isotope analysis was carried out at the State Key Laboratory of Lithospheric Evolution in Institute of Geology and Geophsics, Chinese Academy of Sciences (CAS), Beijing. The detailed analytical protocols and data acquisition method have been described by Xu et al. (2004) and F.-Y. Wu et al. (2006). A Geolas-2005 laser-ablation system equipped with a Neptune multi-collector ICPMS. Typical ablation times were 30 to 90 s with a 10 Hz repetition rate and laser power of 100 mJ, resulting in an ablation depth of ~30 μm. The spot diameter for zircon was 44 μm. The isobaric interference of ^{176}Lu and ^{176}Yb on ^{176}Hf was corrected following the method described in Iizuka and Hirata (2005). During the analysis, the standard zircons Monastery and GJ-1 gave ^{176}Hf/^{177}Hf ratios of 0.282542 ± 0.000016 (2SD, n = 27) and 0.282044 ± 0.000009 (2SD, n = 27), respectively. They are well consistent with the recommended ^{176}Hf/^{177}Hf ratios of 0.282738 ± 0.000004 for Monastery (Woodhead and Hergt, 2005) and 0.282015 ± 0.000019 for GJ-1 (Elhlou et al., 2006) within analytical errors, respectively. All zircon Lu–Hf isotope ratios were measured on adjacent domains for the previous laser U–Pb dating. The Lu–Hf isotope results are reported with the error in 2σ of the mean, and statistical treatment proceeds by the ISOPLOT program of Ludwig (2003).

Initial ^{176}Hf/^{177}Hf ratios were calculated with reference to the chondritic reservoir at the time of zircon growth and by using the U–Pb ages that can clearly define the two independent events of magmatism for inherited domains and metamorphism for new growths (Zheng et al., 2005). In this study, they are the age of discordia upper and lower intercepts, respectively. The $\varepsilon_{Hf}(t)$ values are defined as the 0.1% difference between the sample and the chondritic reservoir at the time of zircon growth. The decay constant for ^{176}Lu of 1.865×10^{-11} yr. (Scherer et al., 2001), the chondritic ratios of ^{176}Hf/^{177}Hf (0.282772) and ^{176}Lu/^{177}Hf (0.0332) were adopted (Blichert-Toft and Albarede, 1997). One-stage Hf model ages (T_{DM1}) are calculated relative to a model depleted mantle with a present-day ^{176}Hf/^{177}Hf ratio of 0.28325 and ^{176}Lu/^{177}Hf of 0.0384 (Griffin et al., 2000), and two-stage Hf model ages (T_{DM2}) are calculated for the source rock by assuming a mean ^{176}Lu/^{177}Hf value of 0.015 for average continental crust (Griffin et al., 2002). Errors of $\varepsilon_{Hf}(t)$ value and Hf model age are calculated on the basis of analytical errors alone, which will be much larger due to the large uncertainties with the reference model (Zheng et al., 2005, 2006).

3.6. Zircon O isotopes

Individual zircon O isotopes were measured using the CAMECA IMS 1270 ion microprobe in a Faraday multicollection mode at University of California at Los Angeles. The detailed analytical protocols and operating conditions have been described by Trail et al. (2007). Instrumental fractionation was calibrated using bracketing and interspersed analyses of zircon standard Qinghu with $\delta^{18}O = 5.39 \pm 0.22$ (2σ; X.H. Li et al., 2013) mounted together with the unknowns. Zircon standard Penglai was analyzed as monitor (Li et al., 2010). The analytical spot size is ca. 20 μm in diameter. The measured ^{18}O/^{16}O ratios were normalized to the VSMOW composition, and then corrected for IMF following Trail et al. (2007). The corrected $\delta^{18}O$ values are reported in the standard per mil notation, along with the 1σ internal errors throughout the text. The obtained $\delta^{18}O$ values for Penglai in this study are 5.28 ± 0.29‰ (n = 14), consistent with the recommended value of 5.31 ± 0.1‰ (2σ; Li et al., 2010).

4. Results

4.1. Geochemistry of jadeite quartzite

The whole-rock major element composition of jadeite quartzite 12DB35 is plotted in the diagram of total alkalis ($K_2O + Na_2O$) vs. SiO_2 (Fig. 4). This sample has high SiO_2, Al_2O_3 and Na_2O contents (Table 1), in agreement with the jadeite- and quartz-dominated mineralogy. The jadeite quartzite contains high concentrations of Zr (506 ppm), Nb (16.8 ppm), Y (45.6 ppm), Ba (13.7 ppm) and Sr (20 ppm) (Fig. 4). Their chondrite-normalized rare earth element (REE) patterns (Fig. 4b) are similar to those of common continental crustal rocks with marked negative Eu anomalies, steep and enriched LREE and relatively flat HREE patterns.

Garnet grains from the jadeite quartzite show relatively homogeneous compositions (Table 2), with mole fractions of 0.61–0.62 for almandine, 0.20–0.21 for pyrope, 0.17–0.18 for grossular, and <0.01 for spessartine. The analyzed jadeites are characterized by high jadeite mole fractions of 0.81–0.83, with aegirine 0.10–0.12 and augite 0.07–0.09 (Table 2).

4.2. Zircon mineragraphy

Zircon grains from the jadeite quartzite 12DB35 are generally anhedral to subhedral, short prismatic, rounded and near-spherical,

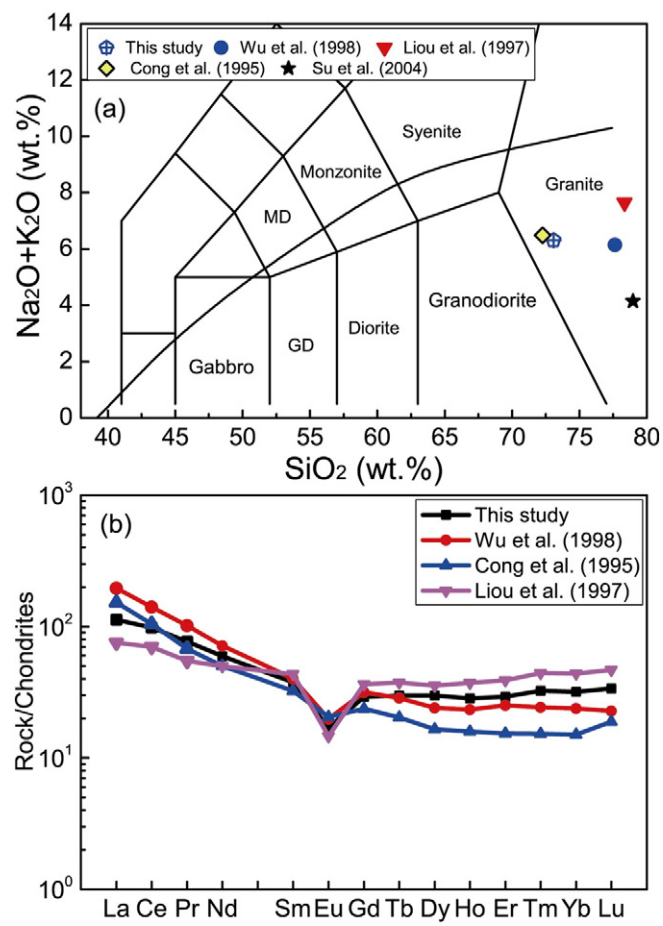

Fig. 4. (a) Total alkalis vs. SiO_2 diagram for jadeite quartzite from Shuanghe in the Dabie orogen. Classifications are after Le Bas et al. (1986). (b) Chondrite-normalized REE patterns for jadeite quartzite. Chondrite values are from Sun and McDonough (1989). MD and GD denote the monodiorite and gabbrodiorite, respectively.

Table 1
Major and trace elements in jadeite quartzite 12DB35 from Shuanghe in the Dabie orogen.

Elements	This study	Wu et al. (1998)	Liou et al. (1997)	Cong et al. (1995)	Su et al. (2004)
Major elements (wt.%)					
SiO_2	73.09	77.63	78.35	72.26	78.98
TiO_2	0.58	0.19	0.08	0.62	0.56
Al_2O_3	12.09	11.95	11.52	12.55	8.32
Fe_2O_3	5.66	1.60	1.89	4.63	3.94
MnO	0.02	0.04	0.09	0.02	0.03
MgO	0.74	0.22	0.06	0.97	1.23
CaO	1.46	0.07	0.28	1.4	1.26
Na_2O	6.28	4.86	3.97	6.35	4.11
K_2O	0.03	1.29	3.67	0.14	0.03
P_2O_5	0.07	0.04	0.04	0.07	0.14
Cr_2O_3	<0.01	nd	nd	nd	nd
SrO	<0.01	nd	nd	nd	nd
BaO	<0.01	nd	nd	nd	nd
LOI	0.02	0.73	nd	0.22	1.02
Total	100.05	98.62	99.95	99.23	99.62
$Na_2O + K_2O$	6.31	6.15	7.64	6.49	4.14
Trace elements (ppm)					
Sc	nd	3	nd	nd	6.57
V	12.0	15	5.84	nd	nd
Cr	50.0	10	12.4	nd	2.14
Co	nd	1.6	nd	nd	1.08
Ni	nd	5	5.92	nd	0.32
Rb	1.60	37	74	nd	29
Sr	20.0	30.8	56.7	nd	22.0
Y	45.6	36.2	nd	nd	24.3
Zr	506	197	202.1	298	424
Nb	16.8	10.6	14.2	14.5	3.48
Ba	13.7	892	480	nd	182
Hf	15.1	6.8	9.1	nd	9.08
Ta	1.20	1.3	4.72	nd	nd
Th	5.43	13.0	9.73	nd	nd
U	1.42	2.03	0.91	nd	nd
La	26.7	46.4	17.9	54.5	36.1
Ce	60.1	86.4	42.9	105	64.3
Pr	7.29	9.67	5.2	nd	6.42
Nd	27.8	33.4	23.3	43.92	23.4
Sm	5.76	6.15	6.65	7.93	4.95
Eu	0.99	1.15	0.85	1.42	1.19
Gd	6.00	6.51	7.49	6.97	4.87
Tb	1.12	1.07	1.4	nd	0.76
Dy	7.58	6.1	9.00	4.1	4.21
Ho	1.61	1.32	2.11	nd	0.9
Er	4.85	4.16	6.45	4.1	2.54
Tm	0.83	0.62	1.13	nd	0.39
Yb	5.42	4.05	7.47	3.67	2.56
Lu	0.86	0.58	1.19	0.56	0.48
REE	157	208	133	nd	153
LREE/HREE	9.0	7.5	2.7	nd	8.2
Eu/Eu*	0.51	0.63	0.37	nd	0.74
La/Yb	4.9	7.5	1.6	nd	nd

Note: "nd" denotes not determined.

ranging from 200 to 600 μm in length with length/width ratios of about 1:1 to 3:1 (Fig. 5). In CL images, most of the zircons show core-rim structures (Fig. 5). There are large cores surrounded by thin rims. The cores are mostly dark-gray with weak luminescence. Generally, most zircon cores were partly disturbed to show faint zoning and/or chaotic zoning, and are commonly embayed by the thin and bright rims.

Raman spectroscopy analyses allow the identification of mineral inclusions in the zircons. The outer bright-luminescent rims preserve rare mineral inclusions, mostly quartz (Fig. 5). The relict zircon cores contain not only significantly UHP mineral inclusions such as coesite, rutile, and jadeite but also multiphase solid (MS) inclusions (Fig. 5c,f). In addition, there are abundant fluid inclusions in the zircon cores (Fig. 5a,d). The MS inclusions occur as isolated ones, indicating their primary property relative to the host zircon. These MS inclusions are so small that can only be found under the optical microscope. They were confirmed by the laser Raman and EDS analyses, showing the compositions of Qz + Kfs, Qz + Kfs + Jd, Qz/Coe + Kfs + Ab + Jd + Bt + Rt

Table 2
Major element compositions of jadeite and garnet from jadeite quartzite 12DB35 at Shuanghe in the Dabie orogen.

Spot	1–1	2–1	3–1	4–2	1–2	2–2	3–2
Mineral	Jd	Jd	Jd	Jd	Grt	Grt	Grt
SiO_2	56.48	56.28	56.56	56.59	39.02	39.12	38.93
TiO_2	0.04	0.06	0.06	0.03	0.03	0.05	0.05
Al_2O_3	22.23	22.56	22.71	22.65	21.47	21.82	21.71
Cr_2O_3	–	–	–	–	0.02	0.03	0.01
FeO	3.63	3.88	4.02	3.53	28.16	27.56	27.84
MnO	–	0.01	0.01	–	0.25	0.32	0.33
MgO	1.34	1.03	0.98	1.10	5.41	5.20	5.32
CaO	2.38	1.94	1.82	2.07	6.02	6.31	6.01
Na_2O	13.82	14.12	13.58	14.00	0.03	0.02	0.03
K_2O	0.04	0.12	0.25	0.01	–	–	–
Total	99.97	99.98	99.98	99.98	100.42	100.44	100.24
O	6	6	6	6	12	12	12
Si	1.93	1.92	1.94	1.93	3.03	3.02	3.02
Ti	–	–	–	–	–	–	–
Al	0.89	0.91	0.92	0.91	1.97	1.99	1.99
Cr	–	–	–	–	–	–	–
Fe^{3+}	0.10	0.11	0.12	0.10	–	–	–
Fe^{2+}	–	–	–	–	1.83	1.81	1.83
Mn	–	–	–	–	0.02	0.02	0.02
Mg	0.07	0.05	0.05	0.06	0.63	0.60	0.62
Ca	0.09	0.07	0.07	0.08	0.50	0.52	0.50
Na	0.91	0.93	0.90	0.93	–	–	–
K	0.00	0.01	0.01	0.00	–	–	–
Jd	80.96	81.95	81.23	83.26			
Aeg	10.35	11.01	11.88	9.63			
Aug	8.69	7.04	6.90	7.11			
Alm					61.22	61.34	61.67
Grs					16.93	17.58	16.82
Pyr					21.24	20.27	20.75
Sps					0.55	0.71	0.73
Uv					0.06	0.09	0.03

Note: The element contents below the detection limit of the electron microprobe analyses are denoted as "–".
Mineral abbreviations are after Whitney and Evans (2010): Alm — almandine, Grs — grossular, Pyr — pyrope, Sps — spessartine, Uv — uvarovite, Jd — jadeite, Aeg — aegirine, and Aug — augite.

(Fig. 5c,f). The distribution of minerals in the composite MS inclusions was further constrained by element mapping (Figs. 6 and 7). The results show heterogeneous Al, Si, K and Na distributions, indicating that the jadeite occurs in margins and cores, and K-feldspar and quartz occur as mixed phases.

4.3. Zircon U–Pb ages and trace elements

The *in-situ* analytical data of zircon U–Pb isotopes and trace elements by the LA-ICPMS are presented in Tables 3 and 4, respectively. Twenty-seven U–Pb analyses were made on 17 grains, including 22 spots on the cores, 5 spots on the rims. The cores show oscillatory or blurred oscillatory zonation in the CL images (Fig. 5). They are mostly associated with discordant U–Pb ages (Fig. 8), in which apparent $^{207}Pb/^{206}Pb$ ages range from 983 to 2045 Ma (Table 3). In contrast, the rims exhibit regular or blurred oscillatory or planar zoning with bright CL images (Fig. 5) and concordant U–Pb ages with apparent $^{206}Pb/^{238}U$ ages of 225 to 246 Ma (Table 3). Taken together, all the U–Pb data can be fit to a discordia line that intersects the concordia curve at 234 ± 18 Ma and 2000 ± 43 Ma (MSWD = 4.1), respectively (Fig. 8).

Chondrite-normalized REE patterns for the cores are different in shape and REE abundance from those for the rims (Fig. 9). The cores are characterized by variably high contents of U (323–1371 ppm), Th (32.0–685 ppm), Nb (4.72–30.8 ppm), Ta (2.28–28.0 ppm) and total REE (408–1941 ppm), generally high Th/U ratios of 0.04 to 0.69 (Tables 3 and 4). The characteristic steep HREE patterns and remarkably negative Eu anomalies (Fig. 9) for the cores indicate that they are of magmatic origin, being inherited from the protolith and thus relict

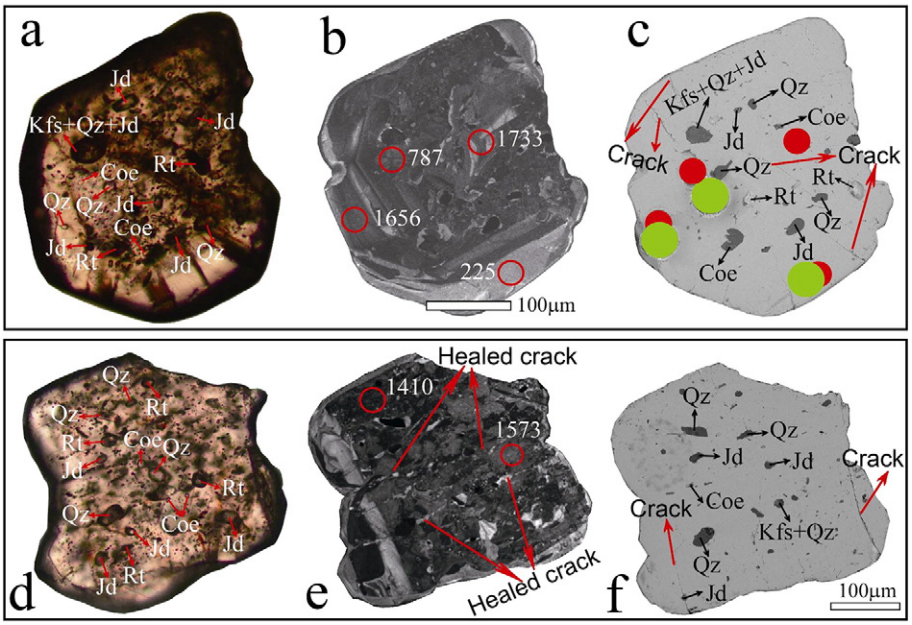

Fig. 5. Plane-polarized light (PPL), CL and BSE images for zircon from jadeite quartzite at Shuanghe in the Dabie orogen. Red circles denote the LA-ICPMS spots (32 μm in diameter) with apparent $^{206}Pb/^{238}U$ ages. Green circles denote the LA-MC-ICPMS spots (44 μm in diameter) with Hf isotope data. (a) The zircon grain contains Jd + Rt + Coe + Qz inclusions in the dusty core and relatively clean metamorphic rim. (b) The CL image for the same zircon as in (a), showing patchy zoned core domains with Precambrian U–Pb ages but bright overgrowth domains with a Triassic U–Pb age. (c) The BSE image for the same zircon as in (a), showing narrow cracks. (d) The zircon grain contains UHP mineral inclusions of Cow + Jd + Rt in the core. (e) The CL image for the same zircon as in (d), with low-luminescent core and very narrow bright rim. (f) The BSE image for the same zircon as in (d), showing several narrow cracks.

domains of detrital origin after metamorphic recrystallization. In contrast, the rims show low element contents, particularly HREE.

4.4. Zircon Lu–Hf isotopes

Twenty-seven LA-MC-ICPMS Lu–Hf isotope analyses were made on 17 zircon grains from the jadeite quartzite (Table 5), which were all dated by the LA-ICPMS U–Pb method (Table 3). The apparent U–Pb ages are positively correlated with $^{176}Lu/^{177}Hf$ ratios but negatively correlated with $^{176}Hf/^{177}Hf$ ratios (Fig. 10a, b). There is also a negative correlation between $^{176}Lu/^{177}Hf$ and $^{176}Hf/^{177}Hf$ ratios (Fig. 10c). The twenty-seven Lu–Hf isotope analyses include 22 spots on the residued cores and 5 spots on the overgrown rims. The initial Hf isotope ratios are calculated at three ages: (1) $t_1 = 2000$ Ma, (2) $t_2 = 230$ Ma, and (3) t = the apparent U–Pb ages (where apparent $^{206}Pb/^{238}U$ ages are taken for the Phanerozoic but apparent $^{207}Pb/^{206}Pb$ ages are taken for the Precambrian in Table 3), respectively.

In general, the newly grown rims are characterized by relatively lower $^{176}Lu/^{177}Hf$ ratios of 0.000034 to 0.000309 and higher $^{176}Hf/^{177}Hf$ ratios of 0.281930 to 0.282446 (Table 5). Their $\varepsilon_{Hf}(t_2)$ values vary from −24.8 to −6.5 at $t_2 = 230$ Ma, corresponding to one-stage Hf model ages (T_{DM1}) of 1113 to 1815 Ma. In contrast, the relict cores show variably high $^{176}Lu/^{177}Hf$ ratios of 0.000091 to 0.001769 and low $^{176}Hf/^{177}Hf$ ratios of 0.281409 to 0.282141 (Table 5). Their $\varepsilon_{Hf}(t_1)$ values vary from −5.0 to 22.3 at $t_1 = 2000$ Ma, corresponding to T_{DM1} ages of 1530 to 2580 Ma. A number of the cores exhibit considerably higher

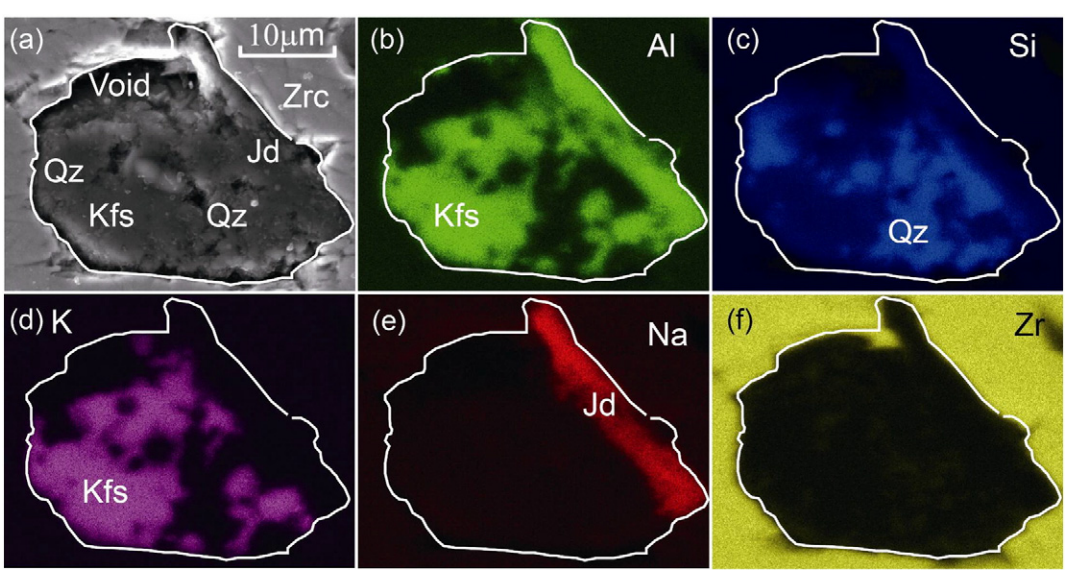

Fig. 6. BSE images and EDS X-ray compositional maps for one multiphase solid inclusion composed of Kfs + Qz + Jd in zircon from the jadeite quartzite at Shuanghe in the Dabie orogen.

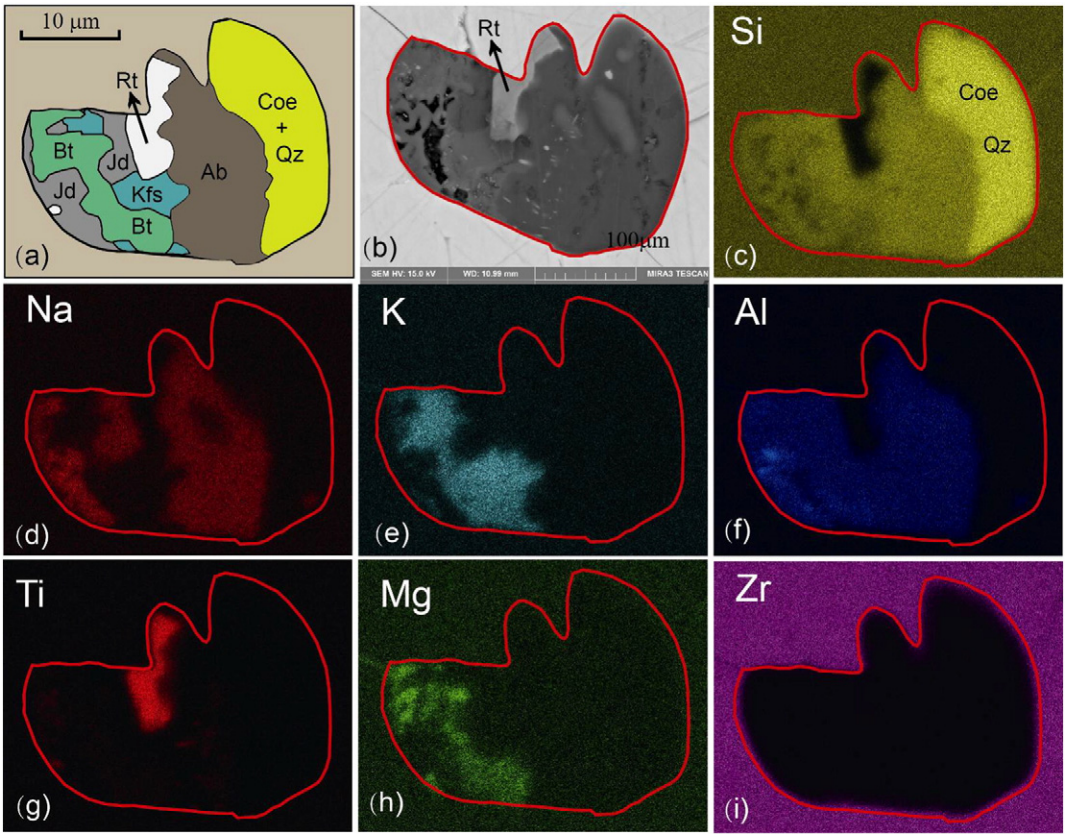

Fig. 7. Sketch images, BSE images and EDS X-ray compositional maps for one multiphase solid inclusion composed of Kfs + Qz/Coe + Jd + Ab + Bt + Rt in zircon from jadeite quartzite from Shuanghe in the Dabie orogen.

$\varepsilon_{Hf}(t_1)$ values calculated at $t_1 = 2000$ Ma than those calculated at t = the apparent U–Pb ages. If we measure this elevation by the relation: $\Delta\varepsilon_{Hf}(t) = \varepsilon_{Hf}(t_1) - \varepsilon_{Hf}(t)$, the relict cores are categorized into two groups (Table 5). The first group shows small deviations of −0.7 to 2.5 (spots #1, #2, #5, #8, #9, #11, #12, #14, #16, #18, #23, #24), whereas the second group exhibits large deviations of 3.7 to 22.9

Table 3
LA-ICPMS analysis of U–Pb isotopes in zircon from jadeite quartzite 12DB35 at Shuanghe in the Dabie orogen.

Spot no.	Type	$^{206}Pb^*$ (ppm)	Th (ppm)	U (ppm)	$\frac{Th}{U}$	Corrected isotope ratios							Apparent ages (Ma)					
						$\frac{^{207}Pb^*}{^{206}Pb^*}$	Error (1σ)	$\frac{^{207}Pb^*}{^{235}U}$	Error (1σ)	$\frac{^{206}Pb^*}{^{238}U}$	Error (1σ)	$\frac{^{207}Pb^*}{^{206}U}$	Error (1σ)	$\frac{^{207}Pb}{^{235}U}$	Error (1σ)	$\frac{^{206}Pb}{^{238}U}$	Error (1σ)
1	I	403	683	995	0.69	0.1227	0.0028	5.31	0.14	0.3084	0.0045	1996	41	1870	134	1733	29
2	I	180	268	480	0.56	0.1254	0.0029	5.13	0.12	0.2928	0.0029	2034	41	1841	115	1656	19
3	II	120	129	806	0.16	0.1102	0.0027	1.99	0.05	0.1291	0.0020	1802	44	1111	52	783	13
4	II	20.7	23.1	353	0.07	0.0719	0.0032	0.537	0.025	0.0534	0.0009	983	90	436	25	335	6
5	II	246	505	897	0.56	0.1156	0.0030	3.28	0.08	0.2030	0.0023	1890	46	1476	82	1191	15
6	III	9.9	5.06	260	0.02	0.0545	0.0034	0.263	0.015	0.0355	0.0006	391	139	237	16	225	4
7	II	134	256	737	0.35	0.1134	0.0032	2.32	0.07	0.1467	0.0019	1854	51	1218	65	882	12
8	I	216	407	973	0.42	0.1171	0.0029	2.80	0.07	0.1713	0.0017	1913	44	1356	67	1019	11
9	I	103	120	386	0.31	0.1169	0.0031	3.49	0.09	0.2141	0.0024	1910	47	1525	89	1251	16
10	III	9.1	3.7	219	0.02	0.0508	0.0035	0.267	0.018	0.0385	0.0007	233	157	240	18	244	5
11	I	140	55.0	635	0.09	0.1154	0.0028	3.08	0.08	0.1912	0.0023	1886	43	1428	75	1128	15
12	I	43.0	51.8	656	0.08	0.1160	0.0040	3.56	0.12	0.2215	0.0031	1895	61	1540	111	1290	20
13	I	182	32.0	647	0.05	0.1117	0.0029	3.81	0.09	0.2446	0.0024	1828	46	1595	91	1410	16
14	I	182	167	534	0.31	0.1201	0.0029	4.62	0.11	0.2763	0.0029	1958	43	1754	104	1573	19
15	III	14.0	6.6	347	0.02	0.0501	0.0027	0.260	0.014	0.0378	0.0005	199	123	235	14	239	3
16	I	108	134	323	0.41	0.1238	0.0029	4.51	0.11	0.2617	0.0027	2011	42	1733	104	1498	18
17	III	8.1	1.6	203	0.01	0.0630	0.0062	0.300	0.030	0.0345	0.0010	456	221	253	26	236	6
18	I	130	79.3	462	0.17	0.1198	0.0034	3.98	0.11	0.2383	0.0023	1954	50	1631	107	1378	15
19	II	63.0	51.3	616	0.08	0.0918	0.0033	1.11	0.04	0.0876	0.0015	1463	68	759	39	541	9
20	II	64.4	50.1	401	0.13	0.1122	0.0034	2.15	0.07	0.1377	0.0014	1836	54	1166	64	831	9
21	II	21.1	17.0	289	0.06	0.0836	0.0038	0.705	0.031	0.0615	0.0009	1283	89	542	31	385	6
22	III	8.3	3.2	189	0.02	0.0501	0.0015	0.272	0.008	0.0389	0.0004	211	101	244	6	246	3
23	I	494	615	965	0.64	0.1261	0.0028	6.82	0.16	0.3885	0.0040	2045	40	2088	146	2116	26
24	I	65.8	55.0	1019	0.05	0.1254	0.0038	5.89	0.18	0.3392	0.0051	2035	53	1960	169	1883	33
25	II	190	43.3	981	0.04	0.1087	0.0027	2.61	0.07	0.1728	0.0023	1777	45	1303	66	1028	15
26	II	246	49.9	1371	0.04	0.1012	0.0025	2.24	0.06	0.1594	0.0019	1646	46	1194	56	953	12
27	I	125	48.5	432	0.11	0.1073	0.0030	3.74	0.10	0.2516	0.0029	1755	52	1580	99	1447	19

Notes: Pb^* indicates the radiogenic portions.

Table 4
LA-ICPMS analysis of trace elements in zircon from jadeite quartzite 12DB35 at Shuanghe in the Dabie orogen.

Spot No.	Ti	Y	Nb	La	Ce	Pr	Nd	Sm	Eu	Gd	Tb	Dy	Ho	Er	Tm	Yb	Lu	Hf	Ta	Nb/Ta	REE	T (°C)
1	22.8	2546	30.8	0.08	51.6	0.11	2.25	5.00	0.52	35.8	15.4	203	81.7	378	81.9	712	129	11,686	11.9	2.58	1696	819
2	5.36	1677	14.6	0.29	26.5	0.16	1.63	3.45	0.38	21.4	9.11	130	53.3	255	54.4	498	84.4	12,343	6.50	2.25	1138	689
3	8.11	682	8.24	bdl	12.2	0.04	0.46	1.11	0.24	7.38	3.47	46.1	20.4	112	26.9	266	49.8	17,221	7.39	1.12	546	723
4	6.51	233	2.29	0.05	8.01	0.03	0.40	1.19	0.39	7.50	2.16	22.8	7.03	32.5	7.39	69.7	14.0	12,988	1.67	1.37	173	705
5	11.8	3073	9.88	0.30	35.0	0.40	4.74	8.83	0.86	49.8	19.5	258	97.8	439	93.4	797	136	10,727	4.22	2.34	1941	756
6	9.23	162	0.99	0.04	4.76	0.03	0.12	0.63	0.40	6.10	2.24	19.2	5.25	17.9	3.19	24.3	4.36	12,990	0.41	2.42	88.5	734
7	15.8	643	14.2	0.08	10.7	0.02	0.36	0.82	0.31	5.03	2.56	40.9	18.6	102	26.7	275	50.7	22,407	28.0	0.51	534	783
8	10.2	904	25.5	0.14	14.8	0.08	0.53	1.55	0.31	7.11	3.58	56.8	25.4	143	37.3	369	69.7	19,526	26.8	0.95	729	743
9	4.02	889	6.67	0.11	14.3	0.07	0.42	1.63	0.29	10.3	4.71	68.9	28.1	141	30.8	287	57.0	10,245	4.61	1.44	645	667
10	11.0	187	1.19	bdl	3.93	bdl	0.21	0.54	0.40	5.59	2.30	22.3	6.02	20.5	3.63	29.1	5.07	12,866	0.45	2.67	100	749
11	13.6	770	10.5	0.07	17.5	0.10	0.15	0.60	0.58	6.42	3.22	48.6	21.2	150	33.2	391	78.8	10,657	10.4	1.01	751	769
12	3.25	673	4.72	bdl	9.54	bdl	0.41	1.47	0.08	8.39	3.64	50.4	21.7	108	23.9	219	39.6	9203	2.28	2.07	487	651
13	13.0	1081	16.2	0.09	25.4	bdl	0.35	0.84	0.30	7.63	4.18	68.4	32.6	225	47.3	520	100	10,302	13.1	1.23	1032	764
14	11.4	880	14.9	0.02	12.7	0.04	1.02	2.20	0.21	10.6	4.71	64.2	27.0	145	35.3	365	73.8	11,506	8.41	1.77	741	753
15	9.09	178	1.52	bdl	4.92	0.02	0.15	0.89	0.49	8.49	2.82	23.2	5.59	17.5	2.93	24.3	4.61	10,545	0.74	2.06	95.9	733
16	5.85	1231	5.64	0.01	13.2	0.13	1.64	3.15	0.22	20.7	7.55	102	40.7	190	40.8	361	65.9	10,311	3.26	1.73	847	696
17	4.12	259	1.41	0.03	4.87	0.03	0.04	0.77	0.42	7.06	2.87	30.4	8.34	28.5	4.47	39.0	6.12	13,862	0.66	2.14	133	669
18	19.7	723	12.9	0.17	14.8	0.17	0.47	0.54	0.52	5.34	2.87	45.1	21.7	158	34.0	392	79.4	11,494	14.1	0.92	755	804
19	13.8	583	5.50	bdl	7.91	0.10	1.45	2.82	0.31	12.8	4.68	51.1	19.6	88.9	20.3	217	52.0	8898	2.67	2.06	479	770
20	18.5	762	8.38	0.05	16.1	bdl	0.37	0.79	0.24	7.01	3.86	53.6	24.3	157	33.2	388	82.9	11,803	8.17	1.03	768	798
21	2.41	322	1.45	bdl	5.05	0.06	0.32	0.89	0.45	9.08	3.07	32.3	10.6	40.2	7.95	63.8	11.8	11,206	0.47	3.11	186	630
22	2.54	198	0.95	bdl	4.08	bdl	bdl	0.75	0.39	5.54	2.30	29.58	6.18	20.5	2.83	27.6	4.33	9177	0.19	5.02	104	633
23	6.54	1969	22.1	bdl	39.6	0.20	1.80	3.66	0.28	23.2	9.22	139	60.4	304	68.3	643	111	13,726	11.7	1.88	1403	705
24	3.54	628	5.59	bdl	11.1	0.02	1.14	2.58	0.10	12.4	4.38	54.6	22.4	102	21.4	205	37.1	7219	3.21	1.74	475	657
25	8.29	470	9.79	0.35	11.5	0.12	0.78	0.67	0.32	3.56	1.99	28.2	14.0	78.1	20.4	210	38.7	8882	9.89	0.99	408	725
26	13.8	547	13.2	0.26	15.8	0.08	0.27	0.90	0.25	5.38	2.30	37.1	15.7	90.0	23.0	253	49.4	9536	15.0	0.88	494	770
27	26.8	503	13.2	0.07	16.1	0.02	0.15	0.45	0.25	4.29	2.30	34.8	14.7	86.2	22.4	234	43.7	10,108	12.6	1.05	460	836

Note: "bdl" denotes contents below the detection limit; temperature was calculated after Ferry and Watson (2007), assuming $a_{TiO2} = 1$ and $a_{SiO2} = 1$.

(spots #3, #4, #7, #13, #19, #20, #21, #25, #26, #27). The large deviations for the second group indicate that it is inappropriate to use $t_1 =$ 2000 Ma for the calculation of their $\varepsilon_{Hf}(t)$ values. Nevertheless, the large deviations are significantly reduced when their $\varepsilon_{Hf}(t)$ values are calculated at t = the apparent $^{207}Pb/^{206}Pb$ ages. This yields $\varepsilon_{Hf}(t)$ values of −7.2 to 2.8 for the second group (Table 5). In this regard, the second group has a different age from the first group.

4.5. Zircon O isotopes

Twenty SIMS *in situ* O isotope analyses were made on fifteen zircon grains from the jadeite quartzite (Table 6). The analytical spots cover different zircon domains, including the relict cores and overgrown rims. The analyses yield $\delta^{18}O$ values of 3.4 to 4.0‰ for the rims and 3.5 to 4.4‰ for the cores. Nevertheless, the $\delta^{18}O$ values for the rims and

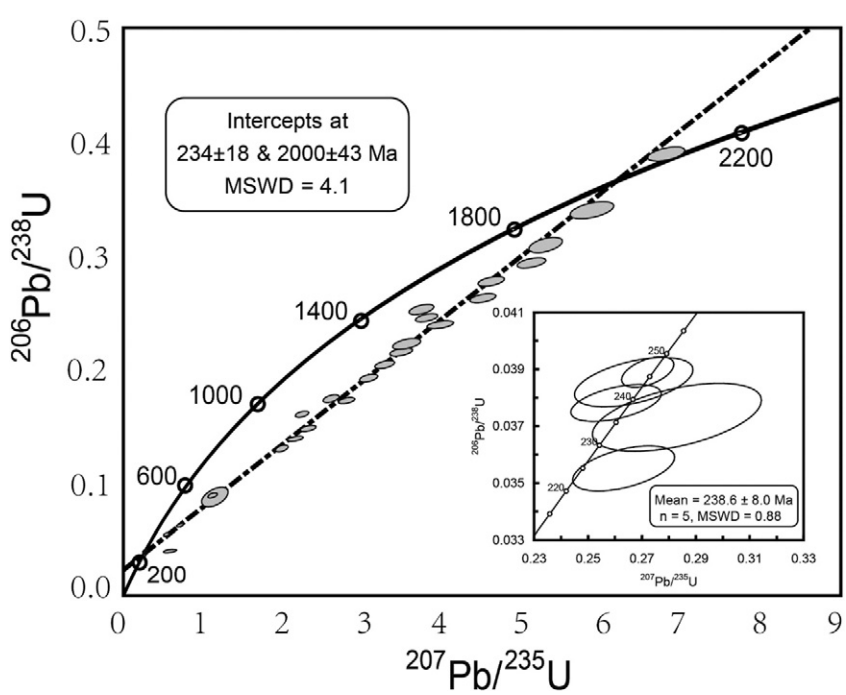

Fig. 8. Concordia diagram of zircon U–Pb dating by LA-ICPMS for the jadeite quartzite from Shuanghe in the Dabie orogen.

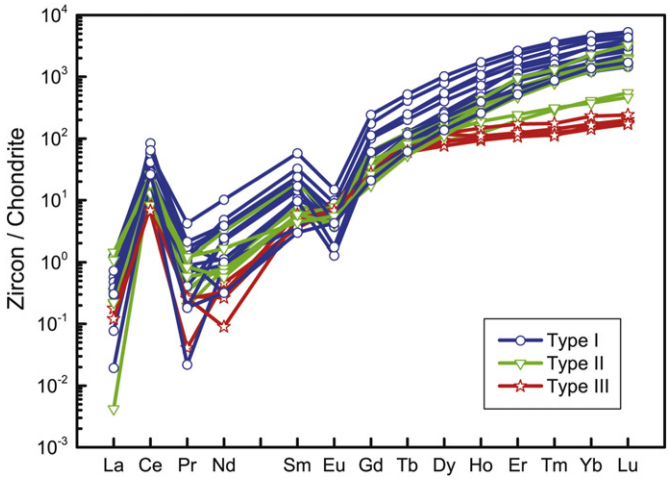

Fig. 9. Chondrite-normalized REE patterns of zircons from the jadeite quartzite at Shuanghe in the Dabie orogen. Chondrite values are after Sun and McDonough (1989).

cores are overlapped with each other within the analytical uncertainties. Taken together, the zircon $\delta^{18}O$ values show a limited range of 3.4 to 4.8‰ with a weighted mean of 4.0 ± 0.2‰. Such values are significantly lower than normal mantle zircon values of 5.3 ± 0.3‰ (Valley et al., 1998).

5. Discussion

5.1. Category of zircons in the jadeite quartzite

Based on an integrated interpretation of the zircon U–Pb ages and trace elements, all the zircon domains from the jadeite quartzite can be categorized into three types (I, II and III). Type-I domains belong to the protolith zircon of magmatic origin and underwent solid-state transformation with the least modification by metamorphic fluids. Thus, they show the nearly full inheritance in U–Pb ages and trace elements from the protolith zircon. Type-II domains underwent metasomatic alteration, showing variable degrees of reworking on the U–Pb isotope and trace element systems by the action of metamorphic fluids. Therefore, Types I and II domains are the metamorphosed zircons due to the different degrees of recrystallization. Type-III domains are metamorphic zircon, new growths from metamorphic fluids. They exhibit concordant U–Pb ages, low Th/U ratios and REE contents, and weak to no Eu anomalies.

Type I domains occur in 14 analyses (spots #1, #2, #5, #8, #9, #11, #12, #13, #14, #16, #18, #23, #24 and #27). The U–Pb isotope data plot close to the apparent discordia upper-intercept age of 2000 ± 43 Ma (Fig. 8), yielding apparent $^{207}Pb/^{206}Pb$ ages ranging from 1755 to 2045 Ma (Table 3). These cores are characterized by variably high contents of U (323–1019 ppm), Th (32.0–683 ppm), Nb (4.72–30.8 ppm), Ta (2.28–26.8 ppm) and REE (460–1941 ppm), relatively high Th/U ratios of 0.05 to 0.69 (Tables 3 and 4).

Type II domains occur in 8 analyses (spots #3, #4, #7, #19, #20, #21, #25, and #26). Their U–Pb isotope data are located below the concordia curve, giving relatively young $^{207}Pb/^{206}Pb$ ages ranging from 983 to 1854 Ma (Table 3). Their trace element concentrations exhibit large variations (Table 4, and Figs. 9 and 11). Two analyses (#4 and #21) yield relatively flat HREE patterns and low REE concentrations. These two domains show the youngest apparent $^{207}Pb/^{206}Pb$ ages of 983 and 1283 Ma, and low Th/U ratios of 0.07 and 0.06. Their Th and U contents are also very low, 23.1 and 17 ppm for Th and 353 and 289 ppm for U. The other 6 analyses (spots #3, #7, #19, #20, #25, and #26) yield trace element compositions similar to Type I domains, exhibiting relatively high concentrations of Nb (5.5–14.2 ppm), Ta (2.67–28.0 ppm), Th (43.3–256 ppm), U (401–1371 ppm) and REE (409–767 ppm) with high Th/U ratios of 0.04 to 0.35 (Tables 3 and 4).

Type III domains occur in 5 analyses (spots #6, #10, #15, #17 and #22). They are only located in the rims. The five U–Pb isotope analyses give concordant ages of 225 ± 4 to 246 ± 3 Ma with a weighted mean of 238.6 ± 8.0 Ma ($n = 5$, MSWD = 0.88) (Table 3 and Fig. 9). They exhibit relatively low contents of U (189–347 ppm), Th (1.59–6.63 ppm), Nb (0.96–1.52 ppm), Ta (0.19–0.74 ppm) and REE (89–133 ppm) with low Th/U ratios of 0.01 to 0.06 (Fig. 10). They are characterized by flat

Table 5
LA-MC-ICPMS zircon Lu–Hf isotope data for jadeite quartzite 12DB35 from Shuanghe in the Dabie orogen.

No.	$^{176}Yb/^{177}Hf$	±(2σ)	$^{176}Lu/^{177}Hf$	±(2σ)	$^{176}Hf/^{177}Hf$	±(2σ)	Age (Ma)	$\varepsilon_{Hf}(t)$	$\varepsilon_{Hf}(t_2)$	$\varepsilon_{Hf}(t_1)$	T_{DM1}(Ma)	±(2σ)	$f_{Lu/Hf}$	T_{DM2}(Ma)	$\Delta\varepsilon_{Hf}(t)$
1	0.06299	0.00084	0.001606	0.000018	0.281517	0.000022	1996	−2.0	−39.6	−1.9	2468	31	−0.95	2732	0.1
2	0.04050	0.00062	0.001152	0.000014	0.281508	0.000025	2034	−0.9	−39.8	−1.6	2451	34	−0.97	2714	−0.7
3	0.03059	0.00021	0.001099	0.000009	0.281583	0.000032	1802	−7.2	−41.7	−2.8	2344	44	−0.97	2546	4.4
4	0.00331	0.00004	0.000091	0.000001	0.282141	0.000024	983	−0.7	−17.3	22.3	1530	33	−1.00	1234	22.9
5	0.06433	0.00049	0.001715	0.000007	0.281495	0.000031	1890	−5.2	−40.4	−2.9	2506	43	−0.95	2789	2.4
6	0.00223	0.00002	0.000061	0.000001	0.281930	0.000026	225	−24.9	−24.8	14.8	1815	35	−1.00	1698	39.7
7	0.02012	0.00011	0.000595	0.000002	0.281586	0.000031	1854	−6.1	−41.9	−2.8	2310	42	−0.98	2498	3.3
8	0.01890	0.00013	0.000551	0.000004	0.281409	0.000027	1913	−6.3	−43.3	−4.3	2547	36	−0.98	2880	2.0
9	0.05064	0.00065	0.001769	0.000038	0.281525	0.000035	1910	−3.8	−39.3	−1.9	2467	49	−0.95	2728	1.9
10	0.00236	0.00002	0.000061	0.000001	0.282446	0.000031	244	−6.2	−6.5	33.2	1113	42	−1.00	553	39.3
11	0.03493	0.00048	0.001109	0.000018	0.281412	0.000045	1886	−7.5	−43.2	−5.0	2580	62	−0.97	2920	2.5
12	0.02005	0.00029	0.000535	0.000005	0.281510	0.000038	1895	−3.1	−39.7	−0.7	2409	51	−0.98	2659	2.4
13	0.01585	0.00027	0.000566	0.000004	0.281457	0.000027	1828	−1.8	−36.5	2.0	2483	37	−0.98	2777	3.8
14	0.02892	0.00026	0.000923	0.000009	0.281493	0.000040	1958	−2.8	−40.3	−1.9	2457	55	−0.97	2728	0.9
15	0.00129	0.00002	0.000034	0.000001	0.282001	0.000034	239	−22.0	−22.2	17.4	1718	46	−1.00	1539	39.4
16	0.02823	0.00048	0.000769	0.000010	0.281502	0.000041	2011	−1.1	−40.0	−1.3	2435	56	−0.98	2696	−0.2
17	0.01021	0.00035	0.000309	0.000011	0.282266	0.000035	235	−12.8	−12.9	26.4	1368	48	−0.99	975	39.2
18	0.01840	0.00011	0.000518	0.000002	0.281452	0.000019	1954	0.1	−37.2	1.1	2486	26	−0.98	2784	1.0
19	0.02037	0.00055	0.000722	0.000019	0.281796	0.000052	1463	−2.8	−29.6	9.2	2030	71	−0.98	2048	11.9
20	0.02697	0.00010	0.000934	0.000004	0.281602	0.000050	1836	−6.3	−41.6	−2.7	2308	69	−0.97	2491	3.7
21	0.00991	0.00009	0.000293	0.000004	0.281994	0.000030	1283	0.7	−22.5	16.8	1739	41	−0.99	1576	16.1
22	0.00146	0.00002	0.000038	0.000001	0.282183	0.000038	246	−15.4	−15.8	23.8	1471	52	−1.00	1137	39.3
23	0.04490	0.00022	0.001224	0.000010	0.281474	0.000031	2045	−2.0	−41.1	−2.9	2502	43	−0.96	2794	−1.0
24	0.03443	0.00024	0.000977	0.000004	0.281489	0.000041	2035	−1.3	−40.5	−2.1	2466	56	−0.97	2741	−0.8
25	0.01413	0.00025	0.000427	0.000008	0.281747	0.000052	1777	2.8	−31.3	7.8	2081	71	−0.99	2131	5.0
26	0.03239	0.00036	0.001011	0.000007	0.281656	0.000045	1646	−4.0	−34.6	3.8	2239	62	−0.97	2380	7.8
27	0.01560	0.00018	0.000435	0.000006	0.281448	0.000019	1755	−3.6	−37.0	1.9	2486	26	−0.99	2786	5.5

Notes: (1) Age denotes the apparent U–Pb ages (AT), with $^{206}Pb/^{238}U$ ages for the Phanerozoic but $^{207}Pb/^{206}Pb$ ages for the Precambrian (Table 3); (2) $\varepsilon_{Hf}(t)$ values are calculated at t_1 = 2000 Ma, t_2 = 230 Ma and t = AT, respectively; (3) $\Delta\varepsilon_{Hf}(t) = \varepsilon_{Hf}(t_1) - \varepsilon_{Hf}(t)$.

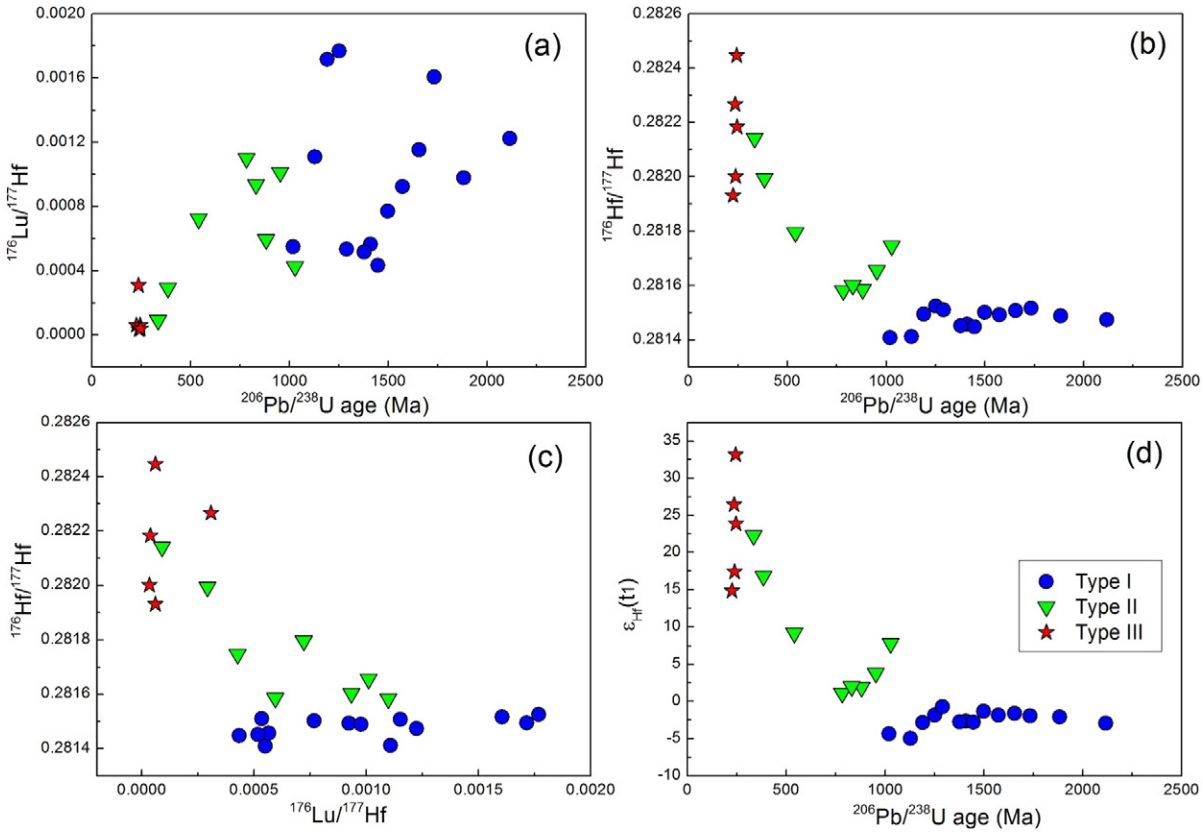

Fig. 10. The relationships between $^{206}Pb/^{238}U$ ages, $^{176}Lu/^{177}Hf$ ratios, $^{176}Hf/^{177}Hf$ ratios and $\varepsilon_{Hf}(t_1)$ values for metamorphosed cores and metamorphic rims in the jadeite–quartzite from Shuanghe in the Dabie orogen. The initial Hf isotope ratios are calculated at $t_1 = 2000$ Ma.

HREE patterns with no Eu anomalies (Fig. 9 and Table 4), typical of metamorphic zircon grown in the garnet stability field (Rubatto, 2002). They show variably low Ti contents of 2.54 to 11.0 ppm, yielding Ti-in-zircon temperatures of 633 to 749 °C (Table 4).

Table 6
SIMS zircon O isotope data for jadeite quartzite 12DB35 from Shuanghe in the Dabie orogen.

Spot	Domain[a]	$^{18}O/^{16}O_m$[b]	1σ (%)[c]	$\delta^{18}O$[d] (‰)	2σ (‰)
12DB35-1	1r	0.00202633	0.014	4.0	0.3
12DB35-2	2c	0.00202534	0.015	3.5	0.3
12DB35-3	3c	0.00202649	0.010	4.1	0.2
12DB35-4	1c	0.00202580	0.006	3.7	0.1
12DB35-6	3r	0.00202623	0.011	3.9	0.2
12DB35-7	4c	0.00202639	0.011	4.0	0.2
12DB35-8	5c	0.00202718	0.012	4.4	0.2
12DB35-9	6c	0.00202540	0.013	3.5	0.3
12DB35-10	7r	0.00202531	0.020	3.5	0.4
12DB35-11	8c	0.00202525	0.010	3.4	0.2
12DB35-12	6r	0.00202642	0.011	4.0	0.2
12DB35-13	9r	0.00202620	0.005	3.9	0.1
12DB35-16	10c	0.00202695	0.011	4.3	0.2
12DB35-17	11r	0.00202801	0.008	4.8	0.2
12DB35-18	12r	0.00202514	0.011	3.4	0.2
12DB35-20	13c	0.00202716	0.012	4.4	0.2
12DB35-22	14c	0.00202688	0.012	4.3	0.2
12DB35-23	13r	0.00202618	0.013	3.9	0.3
12DB35-24	14r	0.00202623	0.010	3.9	0.2
12DB35-25	15c	0.00202642	0.014	4.0	0.3

Notes:
[a] Postfixes c and r denote the core and rim, respectively.
[b] Subscript m denotes the measured $^{18}O/^{16}O$ ratios.
[c] Relative Errors for measured $^{18}O/^{16}O$ ratios.
[d] The $\delta^{18}O$ values have been corrected by the instrumental mass fractionation.

There are also considerable differences in the Lu–Hf isotope composition between the three types of zircon domains (Table 5). Type III domains exhibit $\varepsilon_{Hf}(t)$ values vary from −24.8 to −6.5 at t = 230 Ma, corresponding to one-stage Hf model ages (T_{DM1}) of 1113 to 1815 Ma. In contrast, Type I domains have $\varepsilon_{Hf}(t_1)$ values of −5.0 to 2.0 at t_1 = 2000 Ma, corresponding to one-stage Hf model ages (T_{DM1}) of 2308 to 2580 Ma. The majority of them show small $\Delta\varepsilon_{Hf}(t)$ values of −0.7 to 2.5 (Table 5), suggesting that they only underwent the least degrees of radiogenic Pb loss during the Triassic metamorphism. This is also the reason why their apparent $^{207}Pb/^{206}Pb$ ages of 1755 to 2045 Ma are close to the apparent Discordia upper intercept age of 2000 ± 43 Ma (Fig. 8). On the other hand, Type II domains show $\varepsilon_{Hf}(t)$ values of −7.2 to 2.8, corresponding to T_{DM1} ages of 1530 to 2486 Ma. The majority of them show large $\Delta\varepsilon_{Hf}(t)$ values of 3.7 to 22.9 (Table 5), with younger T_{DM1} ages than <2250 Ma. Their apparent $^{207}Pb/^{206}Pb$ ages of 983 to 1854 Ma are also younger than the apparent discordia upper intercept age of 2000 ± 43 Ma to varying degrees (Fig. 8). In particular, the youngest $^{207}Pb/^{206}Pb$ age of 983 Ma is associated with the youngest T_{DM1} age of 1530 Ma. These observations cannot be explained by the radiogenic Pb loss alone. Instead, Type II domains not only have different ages from Type I domains, but also acquired more radiogenic Hf components from metamorphic fluids. In other words, there is the geochemical mixing between the more and less radiogenic Hf components for the origin of Type II domains.

5.2. Origin of zircons in the jadeite quartzite

Previous studies indicate that zircon may grow or recrystallize under conditions of open or closed systems with variable degrees of fluid action (e.g., Hoskin, 2005; Schaltegger, 2007; Zheng et al., 2007; Chen et al., 2010; Liu and Liou, 2011; Xia et al., 2013). On the one hand, the protolith zircon of magmatic origin may be modified to different extents

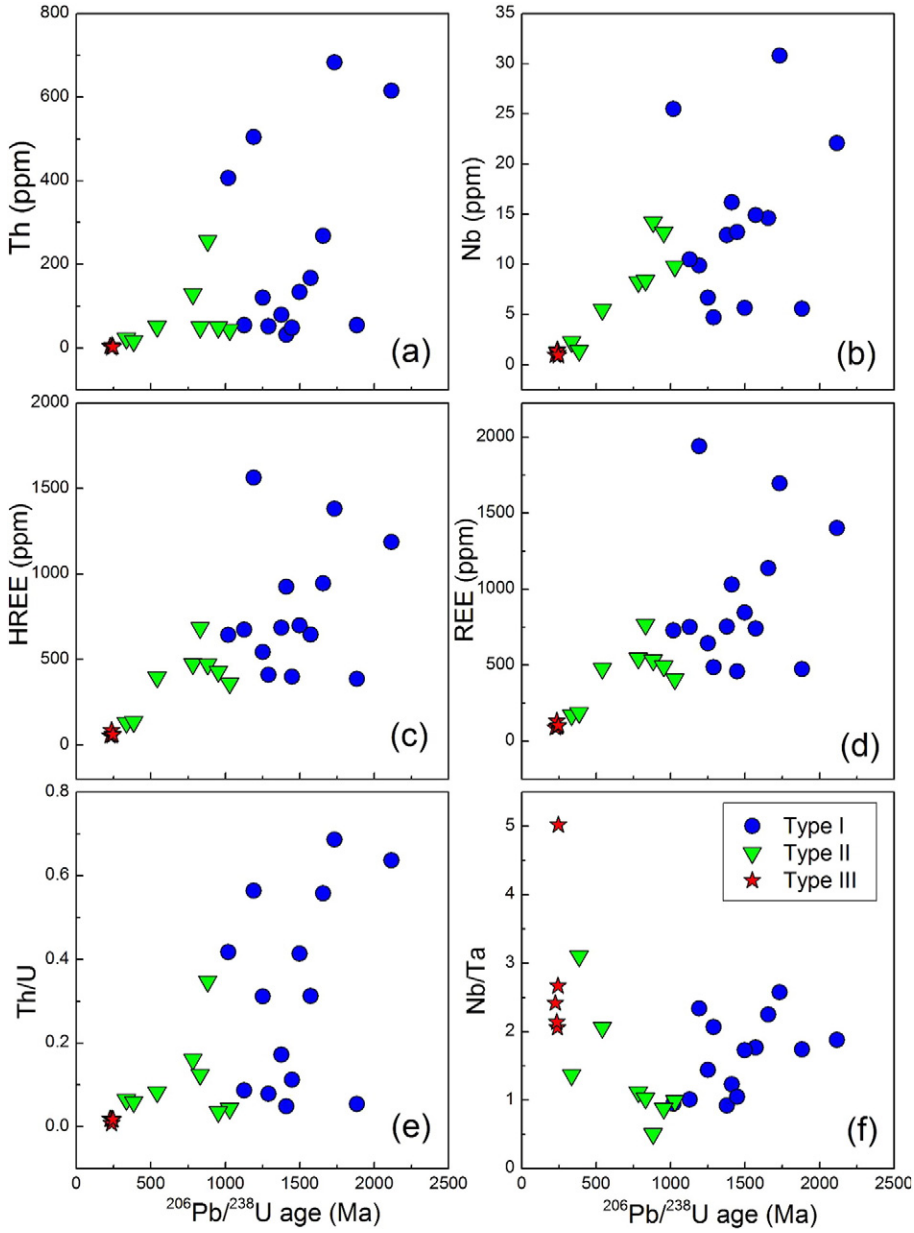

Fig. 11. Plots of apparent U–Pb ages vs. U contents (a), Th contents (b), Nb contents (c), Hf contents (d), total REE (e) and Th/U ratios (f) for metamorphosed cores and metamorphic rims in the jadeite–quartzite from Shuanghe in the Dabie orogen.

via the mechanisms of solid-state transformation, metasomatic alteration and dissolution reprecipitation, depending on the fluid accessibility (Xia et al., 2009, 2010, 2013; Chen et al., 2010, 2011, 2012). The metamorphosed domains commonly occur as the relict cores of magmatic origin, showing discordant U–Pb ages, high Th/U ratios, high REE concentrations and negative Eu anomalies. On the other hand, the metamorphic zircons are new growths from the metamorphic fluids, showing concordant U–Pb ages, low Th/U ratios, low REE concentrations and weak to no Eu anomalies (Zheng, 2009; Chen et al., 2011). According to an integrated interpretation of the all observations for the three types of zircon domains in the jadeite quartzite (Figs. 9, 10 and 11), we are in a position to discriminate between the solid-state recrystallization (Type I), metasomatic recrystallization (Type II) and metamorphic growth (Type III).

Type I domains show high Th/U ratios of 0.05 to 0.69, close to upper-intercept U–Pb ages of 2000 ± 43 Ma, high REE contents of 460 to 1941 ppm, steep REE patterns, high $^{176}Lu/^{177}Hf$ ratios of 0.000435 to 0.001769 and low $^{176}Hf/^{177}Hf$ ratios of 0.281409 to 0.281525 (Tables 3, 4 and 5). In addition, their CL images show the relics of magmatic zircon with partial preservation of the oscillatory zoning. These features indicate that Type I domains would only experience the solid-state recrystallization. In general, the solid-state transformation would only cause the least modification by metamorphic fluids. As a consequence, these domains can still maintain the REE patterns of protolith magmatic zircon but exhibit somewhat younger apparent U–Pb ages. Dissolution reprecipitation of the protolith zircon proceeds during the strongest action of metamorphic fluids, resulting in nearly complete resetting of the protolith U–Pb isotope system and partial reequilibration of the protolith REE systems (Xia et al., 2010).

Type II domains experienced the metasomatic crystallization at the action of metamorphic fluids. This leads to partial modification of the protolith REE, U–Pb and Lu–Hf isotope systems, with possible dissolution reprecipitation of protolith zircon along its fractures and boundaries. Such modification also results in varying degrees of mixing in

trace element and isotope compositions between the protolith zircons and the metamorphic fluids. Thus, the metasomatic products represent the mixtures between protolith zircons and metamorphic fluids (Xia et al., 2009, 2013; Chen et al., 2010, 2011, 2012). As illustrated in Figs. 9, 10 and 11, Type II domains exhibit many features similar to the solid-state recrystallized zircon with respect to their U–Pb ages, trace elements and Lu–Hf isotope compositions. Nevertheless, their U–Pb radiometric system has been modified to different degrees, resulting in variably young $^{206}Pb/^{238}U$ ages than Type I domains (Table 3). The modification is also indicated by the zircon internal structure in that the primary oscillatory zoning was further blurred (or "fade") to patchy or planar zoning (Fig. 5). Similar chaotic and complex secondary textures that cut the primary zones of magmatic zircon are common in hydrothermally altered zircons (e.g., Geisler et al., 2007; Rubatto and Hermann, 2007; Liu et al., 2012). The alteration was attributed to interaction between magmatic zircon and metamorphic fluid (Geisler et al., 2007), and resulted in significant compositional changes, including the loss of radiogenic Pb (Hoskin, 2005; Horie et al., 2006).

Type III domains occur as the rims with high-luminescent CL images (Fig. 5). They are too thin to be analyzed sufficiently. Thus, only five U–Pb isotope analyses were available (Fig. 8). They yield concordant U–Pb ages of 225 ± 4 to 246 ± 3 Ma. These ages overlap with previously obtained dates for eclogite-facies metamorphism of the UHP jadeite quartzite from the same locality (Ayers et al., 2002; Liu et al., 2006). In addition, Type III domains are characterized by unzoned, weakly or cloudy zoned structures in the CL images (Fig. 5), and very low Th contents of 1.59 to 6.63 ppm, U contents of 189 to 347 ppm, and very low Th/U ratios of 0.01 to 0.06 (Fig. 10). These features are typical of metamorphic zircon that grew at eclogite-facies conditions (Rubatto, 2002; Zheng, 2009). Type III domains also show negligible negative Eu anomalies and flat HREE patterns (Fig. 9), indicating their growth in the garnet stability field (Rubatto, 2002; Whitehouse and Platt, 2003). The concordant U–Pb ages of 225 ± 4 to 246 ± 3 Ma are consistent with the UHP metamorphic period of 225 to 240 Ma in the coesite stability field based on previous zircon U–Pb dates for UHP eclogite-facies rocks from the same locality (Zheng et al., 2005; Liu et al., 2006; Y.-B. Wu et al., 2006; Gao et al., 2011). Therefore, the metamorphic zircons in the jadeite quartzite record the action of metamorphic fluid mainly under the UHP eclogite-facies conditions.

In summary, the relict cores in the jadeite quartzite exhibit discordant U–Pb ages (Fig. 8), suggesting that these domains experienced variable extents of metamorphic recrystallization that led to different extents of the Pb loss (Hoskin and Black, 2000; Xia et al., 2009). Type II domains also show somewhat intermediate Hf isotope compositions between Types I and III domains, with high contents of REE similar to Type I domains but comparable Th contents and Th/U ratios with Type III domains (Figs. 9 and 10). This indicates the addition of geochemical components from the metamorphic fluids to the protolith zircons.

5.3. Zircon constraints on the protolith origin of jadeite quartzite

The relict zircon cores in the jadeite quartzite generally show discordant U–Pb ages (Table 3). By fitting to an apparent discordia line, they intersects the Concordia curve at 234 ± 18 Ma and 2000 ± 43 Ma, respectively (Fig. 8). The upper intercept age is consistent with a discordia upper intercept age of 1921 ± 22 Ma measured by the CAMECA ion probe method for zircons from the jadeite quartzite at the same locality (Ayers et al., 2002). The middle Paleoproterozoic age was also acquired from zircons from a number of UHP metamorphic rocks in the Dabie orogen. These include a SHRIMP $^{207}Pb/^{206}Pb$ spot-age of 1861 ± 32 Ma for a pelitic gneiss at Wumiao (Maruyama et al., 1998) and a SHRIMP discordia upper-intercept age of 1817 ± 102 Ma for eclogite at Huangzhen (Li et al., 2004). The premetamorphic protoliths of middle Paleoproterozoic age are evident in the Dabie orogen, suggesting the magmatism of this episode in the northern edge of the South China Block (Zheng et al., 2006). This episode of tectonism is also evident from zircon U–Pb dates for gneisses at Kongling in the Yangtze Gorge (Zhang et al., 2006a; Wu et al., 2009) and granulite and gneiss at Huangtuling in the Dabie orogen (Wu et al., 2008). Therefore, the majority of detrital zircons in the protolith of jadeite quartzite from the Dabie orogen shares the same origin as those contemporaneous magmatic rocks in the South China Block.

Previous studies of major elements in jadeite quartzites from this locality suggest that their protoliths are a kind of sedimentary greywackes (Zhai et al., 1992; Su et al., 1996, 2004; You et al., 1996; Liou et al., 1997; Wang et al., 2010). As such, zircons from the jadeite quartzites would experience weathering and sedimentary cycle, i.e., they are of detrital origin. This is consistent with the present U–Pb isotope dates for the relict zircon cores in the jadeite quartzite from the Dabie orogen. Although the U–Pb data lie along a single discordia line to yield the upper intercept age of 2000 ± 43 Ma (Fig. 8), their apparent U–Pb ages are much more discordant for Type II domains than for Type I domains (Table 3). This difference suggests that the relict zircons in the jadeite quartzite would source from different ages of magmatic rocks. This is confirmed by the difference in zircon Lu–Hf isotope compositions (Table 5).

While zircon U–Pb dating is an important approach to determine the protolith age of metamorphic rocks, zircon Lu–Hf isotope analysis can provide further constraints on the nature of protoliths (Schmidberger et al., 2005; Zheng et al., 2005, 2006). The zircon Lu–Hf isotope analysis yields considerable differences in $^{176}Lu/^{177}Hf$ ratios between rim and core from the jadeite quartzite (Fig. 10), indicating varying degrees of modification by the action of metamorphic fluids on the protolith zircons in the Triassic. To decipher the protolith nature of jadeite quartzite by the zircon Lu–Hf isotopes, it is best to use the relict magmatic zircon domains that only experienced the solid-state recrystallization with the least modification by metamorphic fluids (Zheng et al., 2005, 2006; Xia et al., 2009; Chen et al., 2010, 2014; Beyer et al., 2012). In particular, for relict zircons that only suffered the solid-state recrystallization (Type I domains in the jadeite quartzite), they can inherit the primary Hf isotope composition of protolith magmatic zircons (Zheng et al., 2005, 2006; Flowerdew et al., 2006; Chen et al., 2012, 2013b; Xia et al., 2013).

Although there is a large range in $^{176}Hf/^{177}Hf$ ratios between the different types of zircon domains from the jadeite quartzite (Figs. 9 and 10), such ratios for Type I domains remain relatively homogeneous between 0.281409 and 0.281525 (Fig. 10). This yields $\varepsilon_{Hf}(t)$ values of −7.5 to 0.1 Ma and Hf model ages of 2.31 to 2.58 Ga (Table 5 and Fig. 10). Some granites, migmatites, metasedimentary rocks and amphibolites at the Kongling complex in the northern edge of the South China Block were reported to have zircon U–Pb ages of 1.8–2.0 Ga and negative $\varepsilon_{Hf}(t)$ values (Qiu et al., 2000; Zhang et al., 2006a, 2006b; Xiong et al., 2008; Wu et al., 2009). In the Dabie orogen, nevertheless, these middle Paleoproterozoic rocks were weathered and deposited as the cover of the Neoproterozoic intrusives. On the other hand, Type II domains have $\varepsilon_{Hf}(t)$ values of −7.2 to 2.8 and Hf model ages of 1.53 to 2.49 Ga, suggesting that the protolith of jadeite quartzite contains the detrital zircons from the other ages of magmatic rocks. Taken together, the jadeite quartzite contains the detrial zircons of different U–Pb ages and Hf isotope compositions. This is consistent with the previous conclusion from petrological studies that the sedimentary greywackes are the protolith of jadeite quartzite in the Dabie orogen.

6. Insights into the action of metamorphic fluids on protolith zircon

It is very interesting to note that only Type II domains in the relict cores contain abundant UHP metamorphic single mineral inclusions such as coesite, rutile and jadeite as well as multiphase solid inclusions (Figs. 5, 6 and 7). Evidently, such mineral inclusions were not trapped during crystallization of the protolith magmatic zircons, because pressures for the magma emplacement to crustal levels are typically lower

than 1.0 GPa. Similar inclusions of UHP metamorphic minerals (such as coesite) were observed in relict magmatic zircon domains from UHP metamorphic rocks elsewhere in the world (Gebauer et al., 1997; Zhang et al., 2009; Liu et al., 2012). However, there are different interpretations on the origin of mineral inclusions. In Western Alps, coesite inclusions were sealed within magmatic zircon, which was interpreted to result from successful healing of earlier deformational features, making them "pseudo-inclusion" in relation to the zircon crystal (Gebauer et al., 1997). In this case, SiO_2 must have been introduced along cracks of the magmatic zircon to form the coesite inside it (Gebauer et al., 1997). The similar case was reported from the Dabie-Sulu orogenic belt that was interpreted as the products of fluid metasomatism during the Triassic UHP metamorphism (Zhang et al., 2009; Liu et al., 2012; Xia et al., 2013).

In the jadeite quartzite of our study, the relict coesite and its pseudomorphs occur in the jadeite (Figs. 2 and 3), demonstrating that the jadeite quartzite would have formed under UHP metamorphic conditions. As such, the coesite and UHP mineral inclusions in Type II zircon domains were not magmatic but formed through metasomatism due to fluid infiltrations during the Triassic UHP metamorphism. The existing cracks in zircon are mostly narrow and occur usually in the rims, which cannot be regarded as the primary channel for the fluid infiltration (Fig. 5c,f). Nevertheless, brighter veinlet-like domains filled with abundant mineral inclusions are evident in the CL images for Type II domains, and their irregular boundaries suggest that they represent former cracks (Fig. 5e). Although such cracks had been healed after the fluid action, their presence prior to healing provided possible channels for fluid infiltration into the interior of magmatic zircons. This interpretation is consistent with the observation that abundant mineral inclusions occur along with the healed cracks in Type II domains (Fig. 5e).

Zircon is a petrologically stable and geochemically resistant mineral over a wide P–T range (Rubatto and Hermann, 2007). Although UHP metamorphic rocks were partly or completely reequilibrated during exhumation from the mantle depth to the crustal level, peak metamorphic or even prograde mineral inclusions in zircon from these rocks were protected from retrograde reaction. This provides the petrological evidence for an UHP origin. In the present study, however, the relict magmatic zircon domains show ubiquitous resorption phenomena (Fig. 5), indicating the partial dissolution of zircon and other minerals during the UHP metamorphism in the presence of fluids. It is the partial dissolution that results in the formation of such UHP metamorphic minerals as coesite, rutile and jadeite as inclusions in the protolith zircon (Fig. 12). The above observations demonstrate that modification of the relict zircon cores is likely caused by interaction with metamorphic fluids during continental subduction to coesite-stable depths.

As shown in Fig. 10, the measured zircon Lu–Hf isotope ratios are correlated with their apparent U–Pb ages, regardless of the domain types. For instance, $^{176}Hf/^{177}Hf$ ratios generally increase with decreasing their apparent U–Pb ages (Fig. 10b). Correspondingly, there is a negative correlation between the $\varepsilon_{Hf}(t_2)$ values and the apparent U–Pb ages (Fig. 10d). These trends can be explained by the interaction between the relict magmatic zircon of low $\varepsilon_{Hf}(t)$ and the metamorphic fluid of high $\varepsilon_{Hf}(t)$. Although Type III domains show negative $\varepsilon_{Hf}(t_2)$ values of -24.8 to -6.5 at $t_2 = 230$ Ma, which are higher than very negative $\varepsilon_{Hf}(t_2)$ values of -43.2 to -37.0 for Type I domains at $t_2 = 230$ Ma (Table 5). Such differences suggest that the metamorphic rims incorporated more radiogenic Hf than the relict cores. There are two possibilities for the higher $^{176}Hf/^{177}Hf$ ratios in the metamorphic zircon: (1) they crystallized from externally derived fluids that are more juvenile in origin in an open system (Flowerdew et al., 2006; Zheng et al., 2006); (2) they incorporated more radiogenic Hf released from other HREE-rich minerals in a closed system (Zheng et al., 2005; Y.-B. Wu et al., 2006).

The relict magmatic zircon cores are characterized by relatively higher $^{176}Lu/^{177}Hf$ ratios (>0.0004) and lower $^{176}Hf/^{177}Hf$ ratios than the metamorphic rims (Fig. 11). There are significant differences in

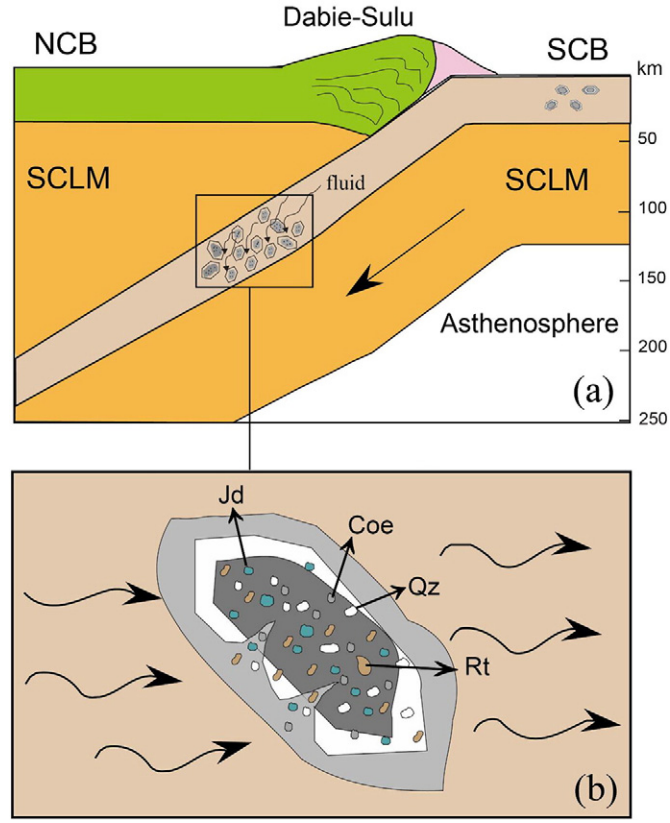

Fig. 12. Schematic cartoon for the formation of metamorphosed zircon domains with amounts of mineral inclusions by fluid metasomatism for the jadeite quartzite in the Dabie orogen. (a) Continental crustal rocks containing magmatic zircon were subducted to the mantle depth for UHP metamorphism, and then exhumed to the crustal level during the collisional orogeny. Metamorphic zircon grew during the continental subduction-zone processes; (b) the UHP mineral inclusions in relict magmatic zircon domains were precipitated from metamorphic fluids infiltrating along microcracks inside the relict magmatic zircon grains. Abbreviations: SCB = the South China Block, NCB = the North China Block, SCLM = subcontinental lithospheric mantle.

the Lu/Hf isotope ratios between the magmatic cores and the metamorphic rims from the same zircon grains, clearly indicating that the metamorphic rims grew from metamorphic fluids that have different Lu–Hf isotope compositions from the magmatic cores. This involves the dissolution of high Lu/Hf minerals (e.g., garnet) into the metamorphic fluids, from which the newly grown rims record the Lu–Hf isotope composition of metamorphic fluids. The existence of garnet during the zircon growth is indicated by the significant decrease in the Lu/Hf isotope ratios for metamorphic zircon (Zheng et al., 2005), which is consistent with the flat HREE patterns for Type III zircon domains (Fig. 9). Therefore, the elevated $\varepsilon_{Hf}(t)$ values for Type III domains are attributable to the incorporation of radiogenic Hf into the metamorphic rims. However, the variably negative $\varepsilon_{Hf}(t_2)$ values of -24.8 to -6.5 cannot be explained by a single crustal source. In view of the known $\varepsilon_{Hf}(t_2)$ values for UHP metamorphic rocks in the Dabie orogen (Zheng et al., 2005, 2006), it is possible that there is the geochemical mixing between ancient and juvenile crustal Hf components in the source of metamorphic fluids.

On the other hand, there are relatively homogeneous $\delta^{18}O$ values for the different types of zircon domains (Table 6), indicating that the metamorphic fluids of interest have the nearly same O isotope composition. The internal origin for metamorphic fluids is consistent with results from previous mineral hydrogen and oxygen isotope studies of UHP metamorphic minerals from the Dabie-Sulu orogenic belt (Zheng et al., 2003, 2009). If any external fluid could be involved in the new

growth of metamorphic rims, such an external fluid would also have similar $\delta^{18}O$ values to the internal fluid. As such, it is not necessary to have the external fluid of similar $\delta^{18}O$ values either for the growth of metamorphic rims or for the recrystallization of protolith zircons. For zircon formed by the dissolution reprecipitation of pre-existing zircon in a closed system, on the other hand, it can inherit the rock Hf isotope composition by the mass balance of Hf element and its isotopes between protolith zircon and rock matrix (Zheng et al., 2005, 2006). In this regard, the trace element and Hf-O isotope characteristics of metamorphic zircon can be used to link their formation to metamorphic conditions.

The metamorphic zircons in the jadeite quartzite are unzoned, with weakly or cloudy zoning structure (Fig. 5). They have very low Th contents of 3.21 to 6.63 ppm and U contents of 189 to 347 ppm, with Th/U ratios as low as 0.03 (Table 4 and Fig. 11). The flat HREE patterns and low Th/U ratios indicate that these zircon domains are of eclogite-facies metamorphic origin (Rubatto, 2002; Zheng, 2009). Although the occurrence of Kfs + Qz, Qz + Kfs + Jd, Qz/Coe + Kfs + Ab + Jd + Bt + Rt MS inclusions in the relict zircon domains (Figs. 5, 6 and 7) may indicate the presence of partial melting (Zeng et al., 2009; Zheng et al., 2011; Gao et al., 2012), no hydrous melts can be inferred from the trace element record in the metamorphic growths. This suggests that the partial melting of UHP metamorphic rocks is of very low extents. In this case, the anatectic melts were confined to grain boundaries, and thus not connected and transported to a long distance.

All the above features indicate that the metasomatism, produced by influx of the metamorphic fluids, occurred at the UHP metamorphic conditions (Fig. 12). Substantially, the existence of such metamorphic fluids has been documented by the study of fluid inclusions and mineral water in jadeite grains of the jadeite–quartzite from this locality (Fu et al., 2001; Su et al., 2004). The UHP mineral inclusions in the relict magmatic zircon domains were crystallized from the metamorphic fluids that were infiltrated along microcracks in the relict magmatic zircon (Fig. 5). The analysis of mineral inclusions and the geochemical characteristics of zircon domains make it possible to identify the timing of fluid metasomatism in the jadeite quartzite, i.e., in the middle Triassic. The mineral inclusions in the relict magmatic cores partly record the composition of UHP metamorphic fluids. In addition, the jadeite quartzite experienced retrogression in view of the pertographic observations, indicating the significant action of metamorphic fluids. The occurrence of mineral inclusions composed of rutile + coesite + jadeite in the relict magmatic zircon domains indicates that the fluids are enriched in SiO_2, Al_2O_3, Na_2O and TiO_2. It is the fluid metasomatism of some Dabie-Sulu UHP metamorphic rocks during the continental subduction to the mantle depth that has partly modified the magmatic zircon cores and reset their isotopic system.

7. Implications for petrogenesis of jadeite quartzite

Generally, jadeite was originally considered as a common mineral in blueschist-facies metamorphic rocks of oceanic subduction zones (Shi et al., 2005; Compagnoni et al., 2007; García-Casco et al., 2009; Harlow et al., 2011; Schertl et al., 2012). However, it also occurs as an important mineral in other metamorphic rocks such as metagranites, metatrachytes and some metasomatic rocks (Chopin, 1984; Hirajima and Compagnoni, 1993; Compagnoni et al., 2007, 2012). Jadeitites and jadeite-bearing rocks are commonly associated with metamorphic rocks produced in subduction channels, for instance, serpentinite formed by antigorite serpentinization of peridotite, presumably from the overlying mantle wedge (Harlow et al., 2015). Previous studies suggested the following two mechanisms for jadeitite petrogenesis (Harlow et al., 2007, 2015): (1) direct precipitation from metamorphic fluids in subduction channels by crustal dehydration into the overlying mantle wedge; (2) metasomatic replacement by metamorphic fluids derived from dehydration of oceanic plagiogranite, greywacke or metabasite along subduction channels. The first mechanism is referred as "P-type" and the second mechanism is referred as "R-type" in the literature. In either case, the metamorphic fluids are required for the both metasomatism and precipitation. Dehydration of deeply subducted crustal rocks at the slab-mantle interface is responsible for the origin of metamorphic fluids.

Most jadeitites and jadeite-rich lithologies in subduction zones would directly crystallize from high-pressure metamorphic fluids with considerable geochemical modification of protoliths (e.g., Tsujimori et al., 2005; Harlow et al., 2007; Tsujimori and Harlow, 2012; Yui et al., 2010; Schertl et al., 2012). As such, the fluid flux in the subduction zones provides important information on the petrogenesis of jadeitites and jadeite-rich lithologies. Previous studies of the jadeite quartzite from the Dabie orogen suggest that their protolith is a kind of sedimentary greywackes (Zhai et al., 1992; Su et al., 1996, 2004; You et al., 1996; Liou et al., 1997). Although the relict zircon cores in the present study show the apparent discordia upper intercept age of 2000 ± 43 Ma (Fig. 8), their $\varepsilon_{Hf}(t_1)$ values would be highly variable if we calculate $\varepsilon_{Hf}(t_1)$ values at t_1 = 2000 Ma for both Types I and II domains (Table 5). However, if we calculate $\varepsilon_{Hf}(t)$ values by taking t = the apparent $^{207}Pb/^{206}Pb$ age, we obtain relatively narrow $\varepsilon_{Hf}(t)$ values of −7.2 to 2.8 for Type II domains (Table 5 and Fig. 11). This suggests that Type II domains have different sources from Type I domains. Therefore, the integrated interpretation of zircon U–Pb ages and Hf isotope compositions indicates that the protolith of jadeite quartzite would be derived from weathering of different ages of magmatic rocks. The magmatic rocks would be physically weathered and then sedimented as the greywackes in a foreland basin prior to the continental collision between the South China Block and the North China Block in the Triassic. The greywackes underwent the UHP metamorphism in the Triassic.

The presence of UHP metamorphic mineral inclusions such as coesite, jadeite and rutile in Type II zircon domains is prominent. Along with the features of trace elements, U–Pb ages and Hf-O isotopes in the zircons, it appears that the metasomatism, produced by the influx of metamorphic fluids, would have occurred at UHP metamorphic conditions. The composition of mineral inclusions in the relict zircon cores indicates that the metamorphic fluids were rich in Si, Ti, Na and Al. The greywacke would be metamorphosed to contain such hydrous minerals as chlorite, amphibole, muscovite and biotite during prograde subduction to the continental lower crustal depth. With further subduction to the mantle depth, these hydrous minerals would break down to release aqueous fluids. Such fluids are of internal origin and would be produced at the tectonic transition from HP to UHP eclogite facies during the final subduction. As outlined by Yui et al. (2010), there are at least two geochemical requirements for the fluid when participating the jadeitite and jadeite-rich rocks: (1) the fluid would be alkalic, capable of dissolving a substantial amount of Al, Na, Zr and Hf; (2) the fluid would be reducing, with divalent Eu, Sr and Ba deriving from decomposition of feldspar and mica. Therefore, we propose that the jadeite quartzite in the Dabie orogen was formed during the UHP metamorphism in the Triassic, and the metasedimentary protolith underwent metasomatic interaction with the metamorphic fluids released from the breakdown of hydrous minerals during the continental subduction-zone metamorphism.

The different zircon domains in the jadeite quartzite show relatively low $\delta^{18}O$ values of 3.4 to 4.8‰ with a weighted mean of 4.0 ± 0.2‰ (Table 6). Because these zircon $\delta^{18}O$ values are significantly lower than the normal mantle zircon values of 5.3 ± 0.3‰, low $\delta^{18}O$ fluids are required to serve as a medium not only for the growth of metamorphic zircons but also for oxygen isotope reequilibration with the protolith zircons. As such, not only Type III domains were precipitated from the low $\delta^{18}O$ fluids in the Triassic, but also Type I and Type II domains were reequilibrated with the low $\delta^{18}O$ fluids during the Triassic UHP metamorphism. Such low $\delta^{18}O$ fluids would have an internal origin, because similarly low $\delta^{18}O$ values of −4.3 to −1.2 are common for metamorphic and metamorphosed zircons from the UHP granitic orthogneiss at Shuanghe in the Dabie orogen (Zheng et al., 2004). In contrast, there are higher $\delta^{18}O$ values of 5 to 10‰ for UHP biotite paragneiss and its associated eclogite at Shuanghe (Zheng et al., 1998; Fu et al., 1999; Zhang et al.,

2003). In this regard, the low $\delta^{18}O$ fluids were derived from dehydration of the UHP granitic orthogneiss during the Triassic subduction-zone metamorphism. The metagreywackes were metasomatized by the metamorphic fluids derived from dehydration of the underlying low $\delta^{18}O$ orthogneiss. Nevertheless, there is the Hf-O isotope decoupling in the three types of zircon domains.

The high $\delta^{18}O$ values of >5‰ are expected for the metagreywacke, the protolith of jadeite quartzite at Shuanghe in the Dabie orogen. But they were reduced to the low $\delta^{18}O$ values of 3.5 to 4.4‰ due to the metasomatism by the low $\delta^{18}O$ metamorphic fluids. In this regard, the fluid metasomatism is evident for the protolith of jadeite quartzite. In doing so, the lower layer of the subducting crust is the source of metamorphic fluids, whereas its upper layer serves as a sink of the metamorphic fluids. This is consistent with geological observations that the subducted continental crust was composed of the sedimentary cover (protoliths of the biotite paragneiss and jadeite quartzite) and the crystalline basement (protolith of the granitic orthogneiss). The metamorphic fluids for the formation of jadeite quartzite were derived from dehydration of the underlying basement orthogneiss during the Triassic UHP metamorphism. While silica-saturated fluids are sufficient for quartz precipitation, the saturation of Si, Al and Na in the metamorphic fluids is necessary for jadeite precipitation. The dissolution of Na and Al from the basement rocks into the metamorphic fluids may be the key to the jadeite formation. Therefore, the jadeite quartzite would have precipitated from the metamorphic fluids that were reacted with the metagreywacke during their migration upwards towards the slab-mantle interface in the continental subduction channel. Consequently, the protolith zircons of detrial origin underwent the varying extents of metamorphic recrystallization during the fluid metasomatism.

8. Conclusions

(1) Zircons in the UHP jadeite quartzite from the Dabie orogen record fluid metasomatism during continental subduction-zone metamorphism. Protolith zircons underwent the metamorphic recrystallization via the mechanisms of solid-state transformation and metasomatic alteration, respectively. The metamorphic zircon grew from aqueous fluids during the metamorphism.

(2) The mineral inclusions of coesite, jadeite and rutile only occur in the metasomatically recrystallized zircons. The protolith zircon of magmatic origin were modified by metamorphic fluids along fractures and the UHP paragenesis of mineral inclusions was formed in these fractures during their healing in response to the metasomatic recrystallization of protolith zircon under the UHP conditions.

(3) The solid-state recrystallized zircons have inherited geochemical signatures from the protolith zircon. Although an apparent U–Pb discordia upper-intercept age of 2000 ± 43 Ma is obtained for relict zircon cores, Lu–Hf isotope data indicates that the magmatic rock of middle Paleoproterozoic age is only a major source for the protolith of jadeite quartzite. In addition, the other source of young rocks was also involved. These different ages of magmatic rocks provide detrital zircons for sedimentary greywackes, the protolith of jadeite quartzite.

(4) The fluid metasomatism of protolith zircons leads to variable extents of modification in both U–Pb and Lu–Hf isotope systems during the UHP metamorphism. While zircon REE composition kept nearly unchanged, zircon O isotope composition was reequilibrated with the metamorphic fluids at the UHP conditions.

(5) The jadeite quartzite in the Dabie orogen was formed by mineral precipitation from the UHP metamorphic fluids during the Triassic subduciton-zone metamorphism. Its metasedimentary protolith was reacted with the metamorphic fluids during the UHP metamorphism, resulting in the dissolution of Na, Al and Si into the fluids for precipitation of the jadeite quartzite. Therefore, there are two-stage processes for the petrogenesis of jadeite quartzite. The fluid metasomatism serves as an important mechanism for enrichment of Na and Al in the metamorphic fluids.

Acknowledgments

This study was supported by funds from the Chinese Ministry of Science and Technology (2015CB856104) and the Natural Science Foundation of China (41572042, 41173046, 41221062 and 41173013). We thank Mei Xia for the mineral SEM-EDS analysis, Shu Zheng for the EMP analysis of mineral major elements, Yongsheng Liu for their assistance with the LA-ICPMS analysis of trace elements and U–Pb ages of zircon, and Yueheng Yang for his assistance with the LA-MC-ICPMS zircon Lu–Hf isotope analysis. Comments by two anonymous reviewers helped the improvement of the presentation. We thank Dr. Klaus Mezger for his editorial handling.

References

Andersen, T., 2002. Correction of common lead in U–Pb analyses that do not report ^{204}Pb. Chem. Geol. 192, 59–79.

Ayers, J.C., Dunkle, S., Gao, S., Miller, C.E., 2002. Constraints on timing of peak and retrograde metamorphism in the Dabie Shan ultrahigh-pressure metamorphic belt, east-central China, using U-Th-Pb dating of zircon and monazite. Chem. Geol. 186, 315–331.

Beyer, E.E., Brueckner, H.K., Griffin, W.L., O'Reilly, S.Y., 2012. Laurentian provenance of archean mantle fragments in the Proterozoic Baltic crust of the Norwegian caledonides. J. Petrol. 53, 1357–1383.

Blichert-Toft, J., Albarede, F., 1997. The Lu–Hf geochemistry of chondrites and the evolution of the mantle-crust system. Earth Planet. Sci. Lett. 148, 243–258 (Erratum, 154, 349).

Bröcker, M., Keasling, A., 2006. Ionprobe U–Pb zircon ages from the high-pressure/low-temperature melange of Syros, Greece: age diversity and the improtance of pre-Eocene subduction. J. Metamorph. Geol. 24, 615–631.

Carswell, D.A., O'Brien, P.J., Wilson, R.N., Zhai, M., 1997. Thermobarometry of phengite-bearing eclogites in the Dabie mountains of central China. J. Metamorph. Geol. 15, 239–252.

Chen, R.-X., Zheng, Y.-F., Xie, L.W., 2010. Metamorphic growth and recrystallization of zircon: distinction by simultaneous in-situ analyses of trace elements, U–Th–Pb and Lu–Hf isotopes in zircons from eclogite-facies rocks in the Sulu orogen. Lithos 114 (1–2), 132–154.

Chen, Y.-X., Zheng, Y.-F., Chen, R.X., Zhang, S.B., Li, Q.L., Dai, M.N., Chen, L., 2011. Metamorphic growth and recrystallization of zircons in extremely ^{18}O-depleted rocks during eclogite-facies metamorphism: evidence from U–Pb ages, trace elements, and O-Hf isotopes. Geochim. Cosmochim. Acta 75 (17), 4877–4898.

Chen, R.-X., Zheng, Y.-F., Hu, Z.C., 2012. Episodic fluid action during exhumation of deeply subducted continental crust: geochemical constraints from zoisite–quartz vein and host metabasite in the Dabie orogen. Lithos 155, 146–166.

Chen, Y.-X., Zheng, Y.-F., Hu, Z., 2013a. Synexhumation anatexis of ultrahigh-pressure metamorphic rocks: petrological evidence from granitic gneiss in the Sulu orogen. Lithos 156-159, 69–96.

Chen, Y.-X., Zheng, Y.-F., Hu, Z., 2013b. Petrological and zircon evidence for anatexis of UHP quartzite during continental collision in the Sulu orogen. J. Metamorph. Geol. 31, 389–413.

Chen, Y.-X., Zheng, Y.-F., Li, L., Chen, R.-X., 2014. Fluid-rock interaction and geochemical transport during protolith emplacement and continental collision: a tale from qinglongshan ultrahigh-pressure metamorphic rocks in the Sulu orogen. Am. J. Sci. 314, 357–399.

Chopin, C., 1984. Coesite and pyrope in high-grade blueschists of the western alps: a first record and some consequences. Contrib. Mineral. Petrol. 86, 107–118.

Compagnoni, R., Rolfo, F., Manavella, F., Salusso, F., 2007. Jadeitite in the monviso meta-ophiolite, Piemonte zone, Italian western alps. Period. Mineral. 76, 79–89.

Compagnoni, R., Rolfo, F., Castelli, D., 2012. Jadeitite from the monviso meta-ophiolite, western alps: occurrence and genesis. Eur. J. Mineral. 24, 333–343.

Cong, B., Zhai, M.G., Carswell, D.A., Wilson, R.N., Wang, Q.C., Zhao, Z.Y., Windley, B.F., 1995. Petrogenesis of ultrahigh-pressure rocks and their country rocks at Shuanghe in Dabieshan, central China. Eur. J. Mineral. 7 (1), 119–138.

Dobretsov, N.L., 1963. Mineralogy, petrography and genesis of ultrbasic rocks, jadeitites, and albitites from the borus mountain range (the west sayan). acadamia scientifica USSR (Siberian branch). Proc. Inst. Geol. Geophys. 15, 242–316.

Elhlou, S., Belousova, E., Griffin, W.L., Pearson, N.J., O'Reilly, S.Y., 2006. Trace element and isotopic composition of GJ red zircon standard by laser ablation. Geochim. Cosmochim. Acta 70, 158.

Flowerdew, M.J., Millar, I.L., Vaughan, A.P.M., Horstwood, M.S.A., Fanning, C.M., 2006. The source of granitic gneisses and migmatites in the Antarctic Peninsular: a combined U–Pb SHRIMP and laser ablation HF isotope study of complex zircons. Contrib. Mineral. Petrol. 151, 751–768.

Fraser, G., Ellis, D., Eggins, S., 1997. Zirconium abundance in granulite-facies minerals, with implications for zircon geochronology in high-grade rocks. Geology 25, 607–610.

Fu, B., Zheng, Y.-F., Wang, Z.R., Xiao, Y.L., Gong, B., Li, S.G., 1999. Oxygen and hydrogen isotope geochemistry of gneisses associated with ultrahigh pressure eclogites at Shuanghe in the Dabie mountains. Contrib. Mineral. Petrol. 134, 52–66.

Fu, B., Touret, J.L.R., Zheng, Y.F., 2001. Fluid inclusions in coesite-bearing eclogites and jadeite quartzite at Shuanghe, Dabie Shan (China). J. Metamorph. Geol. 19, 531–547.

Fu, B., Valley, J., Kita, N.T., Spicuzza, M.J., Paton, C., Tsujimori, T., Bröcker, M., Harlow, G.E., 2010. Multiple origins of zircons in jadeitite. Contrib. Mineral. Petrol. 159 (6), 769–780.

Gao, X.-Y., Zheng, Y.-F., Chen, Y.-X., 2011. U–Pb ages and trace elements in metamorphic zircon and titanite from UHP eclogite in the Dabie orogen: constraints on P–T–t path. J. Metamorph. Geol. 29, 721–740.

Gao, X.-Y., Zheng, Y.-F., Chen, Y.-X., 2012. Dehydration melting of ultrahigh-pressure eclogite in the Dabie orogen: evidence from multiphase solid inclusions in garnet. J. Metamorph. Geol. 30 (2), 193–212.

García-Casco, A., Rodríguez, V.A., Cárdenas, P.J., Iturralde-Vinent, M.A., Lázaro, C., 2009. A new jadeitite jade locality (sierra del convento, Cuba): first report and some petrological and archeological implications. Contrib. Mineral. Petrol. 158, 1–16.

Gasparik, T., 1990. Phase relations in the transition zone. J. Geophys. Res. 95, 15751–75769.

Gebauer, D., Schertl, H.P., Brix, M., Schreyer, W., 1997. 35 Ma old ultrahigh-pressure metamorphism and evidence for very rapid exhumation in the Dora maira massif, western alps. Lithos 41, 5–24.

Geisler, T., Ulonska, M., Schleicher, H., Pidgeon, R.T., van Bronswijk, W., 2001. Leaching and differential recrystallization of metamict zircon under experimental hydrothermal conditions. Contrib. Mineral. Petrol. 141, 53–65.

Geisler, T., Schaltegger, U., Tomaschek, F., 2007. Re-equilibration of zircon in aqueous fluids and melts. Elements 3, 43–50.

Gregory, C.J., Buick, I.S., Hermann, J., Rubatto, D., 2009. Mineral-scale trace element and U-Th-Pb age constraints on metamorphism and melting during the petermann orogeny (central Australia). J. Petrol. 50, 251–287.

Griffin, W.L., Pearson, N.J., Belousova, E., Jackson, S.E., van Achterbergh, E., O'Reilly, S.Y., Shee, S.R., 2000. The Hf isotope composition of cratonic mantle: LAM-MC-ICPMS analysis of zircon megacrysts in kimberlites. Geochim. Cosmochim. Acta 64, 133–147.

Griffin, W.L., Wang, X., Jackson, S.E., Pearson, N.J., O'Reilly, S.Y., Xu, X., Zhou, X., 2002. Zircon chemistry and magma mixing, SE China: in-situ analysis of Hf isotopes, Tonglu and Pingtan igneous complexes. Lithos 61, 237–269.

Harlow, G.E., Sorensen, S.S., Sisson, V.B., 2007. Jade. In: Lee, A. (Ed.), The Geology of Gem DepositsShort Course Handbook Series vol. 37. Mineral. Asso. Canada, Θυεβεχ, pp. 207–254.

Harlow, G.E., Sisson, V.B., Sorensen, S.S., 2011. Jadeitite from Guatemala: distinctions among multiple occurrences. Acta Geol. 9, 363–387.

Harlow, G.E., Tsujimori, T., Sorensen, S.S., 2015. Jadeitites and plate tectonics. Annu. Rev. Earth Planet. Sci. 43, 105–138.

Hermann, J., Zheng, Y.F., Rubatto, D., 2013. Deep fluids in subducted continental crust. Elements 9, 281–287.

Hirajima, T., Compagnoni, R., 1993. Petrology of a jadeite-quartz/coesite-almandine-phengite fels with retrograde ferro-nyboite from the Dora-Maria massif, western alps. Eur. J. Mineral. 5 (5), 943–955.

Holland, T.J.B., 1980. The reaction albite = jadeite + quartz determined experimentally in the range 600–1200 °C. Am. Mineral. 65, 129–134.

Horie, K., Hidaka, H., Gauthier-Lafaye, F., 2006. Elemental distribution in zircon: alteration and radiation-damage effects. Phys. Chem. Earth 31, 587–592.

Hoskin, P.W.O., 2005. Trace-element composition of hydrothermal zircon and the alteration of hadean zircon from the jack hills, Australia. Geochim. Cosmochim. Acta 69, 637–648.

Hoskin, P.W.O., Black, L.P., 2000. Metamorphic zircon formation by solid-state recrystallization of protolith igneous zircon. J. Metamorph. Geol. 18, 423–439.

Hoskin, P.W.O., Schaltegger, U., 2003. The composition of zircon and igneous and metamorphic petrogenesis. Rev. Mineral. Geochem. 53 (1), 27–62.

Iizuka, T., Hirata, T., 2005. Improvements of precision and accuracy in situ Hf isotope microanalysis of zircon using the laser ablation-MC-ICPMS technique. Chem. Geol. 220, 121–137.

Jackson, S.E., Pearson, N.J., Griffin, W.L., Belousova, E.A., 2004. The application of laser ablation-inductively coupled plasma-mass spectrometry to in situ U–Pb zircon geochromology. Chem. Geol. 211, 47–69.

Le Bas, M.J., Le Maitre, R.W., Streckeisen, A., Zanettin, B.A., 1986. Chemical classification of volcanic rocks based on the total alkalisilica diagram. J. Petrol. 27, 745–750.

Li, S.G., Jagoutz, E., Lo, C.H., Chen, Y., Li, Q., Xiao, Y., 1999. Sm/Nd, Rb/Sr, and $^{40}Ar/^{39}Ar$ isotopic systematics of the ultrahigh-pressure metamorphic rocks in the Dabie-Sulu belt, central China: a retrospective view. Int. Geol. Rev. 41, 1114–1124.

Li, S.G., Jagoutz, E., Chen, Y.Z., Li, Q.L., 2000. Sm-Nd and Rb-Sr isotopic chronology and cooling history of ultrahigh pressure metamorphic rocks and their country rocks at Shuanghe in the Dabie mountains, central China. Geochim. Cosmochim. Acta 64 (6), 1077–1093.

Li, X.-P., Zheng, Y.-F., Wu, Y.-B., Chen, F.K., Gong, B., Li, Y.-L., 2004. Low-T eclogite in the Dabie terrane of China: petrological and isotopic constraints on fluid activity and radiometric dating. Contrib. Mineral. Petrol. 148, 443–470.

Li, X.H., Long, W.G., Li, Q.L., Liu, Y., Zheng, Y.F., Yang, Y.H., Chamberlain, K.R., Wan, D.F., Guo, C.H., Wang, X.C., Tao, H., 2010. Penglai zircon megacrysts: a potential new working reference material for microbeam determination of Hf–O isotopes and U–Pb age. Geostand. Geoanal. Res. 34 (2), 117–134.

Li, W.-C., Chen, R.-X., Zheng, Y.-F., Li, Q., Hu, Z., 2013a. Zirconological tracing of transition between aqueous fluid and hydrous melt in the crust: constraints from pegmatite vein and host gneiss in the Sulu orogen. Lithos 162-163, 157–174.

Li, X.H., Tang, G.Q., Gong, B., Yang, Y.H., Hou, K.J., Hu, Z.C., Liu, Y., Li, W.X., 2013b. Qinghu zircon: a working reference for microbeam analysis of U–Pb age and Hf and O isotopes. Chin. Sci. Bull. 58, 4647–4654.

Li, W.-C., Chen, R.-X., Zheng, Y.-F., Hu, Z.C., 2014. Dehydration and anatexis of UHP metagranite during continental collision in the Sulu orogen. J. Metamorph. Geol. 32, 915–936.

Liou, J.G., Zhang, R.Y., Jahn, B.M., 1997. Petrology, geochemistry and isotope data on a ultrahigh-pressure jadeite quartzite from Shuanghe, Dabie mountains, east-central China. Lithos 41 (1–3), 59–78.

Liou, J.G., Ernst, W.G., Zhang, R.Y., Tsujimori, T., Jahn, J.G., 2009. Ultrahigh-pressure minerals and metamorphic terranes — the view from China. J. Asian Earth Sci. 35, 199–231.

Liu, F.L., Liou, J.G., 2011. Zircon as the best mineral for P–T-time history of UHP metamorphism: a review on mineral inclusions and U–Pb SHRIMP ages of zircons from the Dabie-Sulu UHP rocks. J. Asian Earth Sci. 40 (1), 1–39.

Liu, D.Y., Jian, P., Kröner, A., Xu, S.T., 2006. Dating of prograde metamorphic events deciphered from episodic zircon growth in rocks of the Dabie–Sulu UHP complex, China. Earth Planet. Sci. Lett. 250 (3–4), 650–666.

Liu, Y.S., Hu, Z.C., Gao, S., Günther, D., Xu, J., Gao, C.G., Chen, H.H., 2008. In situ analysis of major and trace elements of anhydrous minerals by LA–ICP–MS without applying an internal standard. Chem. Geol. 257, 34–43.

Liu, Y.S., Hu, Z.C., Zong, K.Q., Gao, C.G., Gao, S., Xu, J., Chen, H.H., 2010. Reappraisement and refinement of zircon U–Pb isotope and trace element analyses by LA–ICP–MS. Chin. Sci. Bull. 55, 1535–1546.

Liu, F.L., Gerdes, A., Liu, P.H., 2012. U–Pb, trace element and Lu–Hf properties of unique dissolution–reprecipitation zircon from UHP eclogite in SW Sulu terrane, eastern China. Gondwana Res. 22 (1), 169–183.

Ludwig, K.R., 2003. ISOPLOT 3.00: a geochronological toolkit for Microsoft excel. Berkeley Geochronology Center, California, Berkeley.

Martin, L.A.J., Duchene, S., Deloule, E., Vanderhaeghe, O., 2008. Mobility of trace elements and oxygen in zircon during metamorphism: consequences for geochemical tracing. Earth Planet. Sci. Lett. 267, 161–174.

Maruyama, S., Tabata, H., Nutman, A.P., Morikawa, T., Liou, J.G., 1998. SHRIMP U–Pb geochronology of ultrahigh-pressure metamorphic rocks of the dabie mountains, central China. Cont. Dyn. 3, 72–85.

Möller, A., O'Brien, P.J., Kennedy, A., Kroner, A., 2003. Linking growth episodes of zircon and metamorphic textures to zircon chemistry: an example from the ultra-high temperature granulites of Rogaland (SW Norway). Geol. Soc. Spec. Publ. 220, 65–81.

Okay, A.I., 1993. Petrology of a diamond and coesite-bearing metamorphic terrane: Dabie Shan, China. Eur. J. Mineral. 5, 659–673.

Okay, A.I., Xu, S.T., Sengor, A.M.C., 1989. Coesite from the Dabie Shan eclogites, central China. Eur. J. Mineral. 1, 595–598.

Prewitt, C.T., Burnham, C.W., 1996. The crystal structure of Jadeite, $NaAlSi_2O_6$. Am. Mineral. 51, 956–975.

Qiu, Y.M., Gao, S., McNaughton, N.J., Groves, D.I., Ling, W.L., 2000. First evidence of ≥3.2 Ga continental crust in the Yangtze craton of south China and its implications for Archean crustal evolution and Phanerozoic tectonics. Geology 28, 11–14.

Rubatto, D., 2002. Zircon trace element geochemistry: partitioning with garnet and the link between U–Pb ages and metamorphism. Chem. Geol. 184, 123–138.

Rubatto, D., Hermann, J., 2003. Zircon formation during fluid circulation in eclogites (monviso, western alps): implications for Zr and Hf budget in subduction zones. Geochim. Cosmochim. Acta 67, 2173–2187.

Rubatto, D., Hermann, J., 2007. Zircon behavior in deeply subducted rocks. Elements 3, 31–35.

Schaltegger, U., 2007. Hydrothermal zircon. Elements 3, 51–79.

Scherer, E., Munker, C., Mezger, K., 2001. Calibration of the lutetium-hafnium clock. Science 293, 683–687.

Schertl, H.-P., Schreyer, W., 2008. Geochemistry of coesite-bearing "pyrope quartzite" and related rocks from the Dora-Maira massif, western Alps. Eur. J. Mineral. 20, 791–809.

Schertl, H.P., Maresch, W.V., Stanek, K.P., Hertwig, A., Krebs, M., Baese, R., Sergeev, S.S., 2012. New occurrences of jadeitite, jadeite quartzite and jadeite-lawsonite quartzite in the Dominican Republic, Hispaniola: petrological and geochronological overview. Eur. J. Mineral. 24, 199–216.

Schmidberger, S.S., Heaman, L.M., Simonetti, A., Creaser, R.A., Cookenboo, H.O., 2005. Formation of paleoproterozoic eclogitic mantle, slave province (Canada): insights from in-situ Hf and U–Pb isotopic analyses of mantle zircons. Earth Planet. Sci. Lett. 240, 621–633.

Shi, G.H., Stöckhert, B., Cui, W.Y., 2005. Kosmochlor and chromian jadeite aggregates from the Myanmar jadeitite area. Mineral. Mag. 69, 1059–1075.

Sobolev, N.V., Dobretsov, N.L., Bakirov, A.B., Shatsky, V.S., 1986. Eclogites from various types of metamorphic complexes in the USSR and problems of their origin. in Blueschists and Eclogites. In: Evans, B.W., Brown, E.H. (Eds.), Geol. Soc. Am. Mem. 16, 349–363.

Su, W., Xu, S., Jiang, L., Liu, Y., 1996. Coesite from the quartz –jadeitite, eastern China. Mineral. Mag. 60, 659–662.

Su, W., Ji, Z.P., Ye, K., You, Z.D., Liu, J.B., Yu, J., Cong, B.L., 2004. Distribution of hydrous components in jadeite of the Dabie mountains. Earth Planet. Sci. Lett. 222 (1), 85–100.

Sun, S.-s., McDonough, W.F., 1989. Chemical and isotopic systematics of oceanic basalts: implications for mantle composition and processes. Geol. Soc. Lond. Spec. Publ. 42, 313–345.

Trail, D., Mojzsis, S.J., Harrison, T.M., Schmitt, A.K., Watson, E.B., Young, E.D., 2007. Constraints on Hadean zircon protoliths from oxygen isotopes, Ti thermometry, and rare earth elements. Geochem. Geophys. Geosyst. 8, Q06014.

Tsai, C.H., Liou, J.G., 2000. Eclogite-facies relics and inferred ultrahigh-pressure metamorphism in the north Dabie complex, central-eastern China. Am. Mineral. 85, 1–8.

Tsujimori, T., Harlow, G.E., 2012. Petrogenetic relationships between jadeitite and associated high-pressure and low-temperature metamorphic rocks in worldwide jadeitite localities: a review. Eur. J. Mineral. 24, 371–390.

Tsujimori, T., Liou, J.G., Wooden, J., Miyamoto, T., 2005. U–Pb dating of large zircons in low-temperature jadeitite from the osayama serpentinite mélange, southwest Japan: insights into the timing of serpentinization. Int. Geol. Rev. 47, 1048–1057.

Valley, J.W., Chiarenzelli, J.R., McLelland, J.M., 1994. Oxygen isotope geochemistry of zircon. Earth Planet. Sci. Lett. 126 (4), 187–206.

Valley, J.W., Kinny, P.D., Schulze, D.J., Spicuzza, M.J., 1998. Zircon megacrysts from kimberlite: oxygen isotope variability among mantle melts. Contrib. Mineral. Petrol. 133 (1), 1–11.

Wang, X.M., Liou, J.G., Mao, H.K., 1989. Coesite-bearing eclogite from the Dabie mountains in central China. Geology 17, 1085–1088.

Wang, X.M., Zhang, R.Y., Liou, J.G., 1995. UHPM terrane in east central China. In: Coleman, R., Wang, X.M. (Eds.), Ultrahigh Pressure Metamorphism. Cambridge University Press, Cambridge, pp. 356–390.

Wang, L., Jin, Z.M., Kusky, T., 2010. Microfabric characteristics and rheological significance of ultra-high pressure metamorphosed jadeite–quartzite and eclogite from Shuanghe, Dabie mountains, China. J. Metamorph. Geol. 28, 163–182.

Wayne, D.M., Sinha, A.K., 1992. Stability of zircon U–Pb systematics in a greenschist-grade mylonite: an example from the rockfish valley fault zone, central Virginia, USA. J. Geol. 100, 593–603.

Whitehouse, M.J., Platt, J.P., 2003. Dating high-grade metamorphism constraints from rare-earth elements in zircons and garnet. Contrib. Mineral. Petrol. 145, 61–74.

Whitney, D.L., Evans, B.W., 2010. Abbreviations for names of rock-forming minerals. Am. Mineral. 95, 185–187.

Wiedenbeck, M., Alle, P., Corfu, F., Griffin, W.L., Meier, M., Oberli, F., von Quadt, A., Roddick, J.C., Spiegel, W., 1995. Three natural zircon standards for U–Th–Pb, Lu–Hf, trace element and REE analyses. Geostand. Geoanal. Res. 19, 1–23.

Woodhead, J.D., Hergt, J.M., 2005. Preliminary appraisal of seven natural zircon reference materials for in situ Hf isotope determination. Geostand. Geoanal. Res. 29, 183–195.

Wu, W.P., Xu, S.T., Jiang, L.L., Liu, Y.C., Su, W., 1998. Quartz-jadeitite in ultrahigh-pressure metamorphic belt in the Dabie mountains, eastern China. Acta Petrol. Sin. 14, 60–70.

Wu, F.-Y., Yang, Y.-H., Xie, L.-W., Yang, J.-H., Xu, P., 2006a. Hf isotopic compositions of the standard zircons and baddeleyites used in U–Pb geochronology. Chem. Geol. 234, 105–126.

Wu, Y.-B., Zheng, Y.-F., Zhao, Z.F., Gong, B., Liu, X.M., Wu, F.Y., 2006b. U–Pb, Hf and O isotope evidence for two episodes of fluid-assisted zircon growth in marble-hosted eclogites from the Dabie orogen. Geochim. Cosmochim. Acta 70 (14), 3743–3761.

Wu, Y.-B., Zheng, Y.-F., Gao, S., Jiao, W.-F., Liu, Y.-S., 2008. Zircon U–Pb age and trace element evidence for paleoproterozoic granulite-facies metamorphism and archean crustal rocks in the Dabie orogen. Lithos 101, 308–322.

Wu, Y.-B., Gao, S., Gong, H.-J., Xiang, H., Jiao, W.-F., Yang, S.-H., Liu, Y.-S., 2009. Zircon U–Pb ages, trace element and Hf isotope composition of kongling terrane in the Yangtze craton: refining the timing of paleoproterozoic high-grade metamorphism. J. Metamorph. Geol. 27, 461–477.

Xia, Q.-X., Zheng, Y.-F., Yuan, H.L., Wu, F.Y., 2009. Contrasting Lu–Hf and U-Th-Pb isotope systematics between metamorphic growth and recrystallization of zircon from eclogite-facies metagranites in the Dabie orogen, China. Lithos 112, 477–496.

Xia, Q.-X., Zheng, Y.-F., Hu, Z.C., 2010. Trace elements in zircon and coexisting minerals from low-T/UHP metagranite in the Dabie orogen: implications for action of supercritical fluid during continental subduction-zone metamorphism. Lithos 114 (3–4), 385–412.

Xia, Q.-X., Zheng, Y.-F., Chen, Y.X., 2013. Protolith control on fluid availability for zircon growth during continental subduction-zone metamorphism in the Dabie orogen. J. Asian Earth Sci. 67-68, 93–113.

Xiao, Y.L., Hoefs, J., van den Kerkhof, A.M., Li, S.G., 2001. Geochemical constraints of the eclogite and granulite facies metamorphism as recognized in the Rabobazhai complex from north Dabie Shan, China. J. Metamorph. Geol. 19, 3–19.

Xiong, Q., Zheng, J.P., Yu, C.M., Su, Y.P., Tang, H.Y., Zhang, Z.H., 2008. Zircon U–Pb age and Hf isotope of Quanyishang A-type granite in Yichang: signification for the Yangtze continental cratonization in Paleoproterozoic. Chin. Sci. Bull. 54, 436–446.

Xu, S.T., Okay, A.I., Ji, S.Y., Sengor, A.M.C., Su, W., Liu, Y.C., Jiang, L.L., 1992. Diamond from the Dabie Shan metamorphic rocks and its implication for tectonic setting. Science 256, 80–82.

Xu, P., Wu, F.Y., Xie, L.W., Yang, Y.H., 2004. Hf isotopic compositions of the standard zircons for U–Pb dating. Chin. Sci. Bull. 49, 1642–1648.

You, Z., Han, Y., Yang, W., Zhang, Z., Wei, B., Liu, R., 1996. The high-pressure and ultra-high-pressure metamorphic belt in the east Qinling and Dabie mountains, China. China University of Geosciences Press, Wuhan, China, p. 150.

Yui, T.-F., Fukuyama, M., 2015. A revisit to the Yorii jadeite-quartz rock, the Kanto mountains, central Japan: implications for petrogenesis. J. Asian Earth Sci. 108, 58–67.

Yui, T.-F., Maki, K., Usuki, T., Lan, C.Y., Martens, U., Wu, C.M., Wu, T.W., Liou, J.G., 2010. Genesis of Γυατεμαλα jadeitite and related fluid characteristics: insight from zircon. Chem. Geol. 270 (1–4), 45–55.

Zeng, L.S., Liang, F.H., Asimow, P., Chen, F.Y., Chen, J., 2009. Partial melting of deeply subducted continental crust and the formation of quartzofeldspathic polyphase inclusions in the Sulu UHP eclogites. Chin. Sci. Bull. 54, 2580–2594.

Zhai, M., Cong, B., Wang, Q., Li, L., 1992. High-pressure jadeite–quartzite from Dabieshan eclogite belt and its geological implication. Chin. Sci. Bull. 37, 1013–1015.

Zhang, R.Y., Hirajima, T., Banno, S., Cong, B.L., Liou, J.G., 1995. Petrology of ultrahigh-pressure rocks from the southern Su-Lu region, eastern China. J. Metamorph. Geol. 13, 659–675.

Zhang, R.Y., Liou, J.G., Zheng, Y.-F., Fu, B., 2003. Transition of UHP eclogites to gneissic rocks of low-grade amphibolite facies during exhumation: evidence from the Dabie terrane, central China. Lithos 70, 269–291.

Zhang, S.-B., Zheng, Y.-F., Wu, Y.-B., Zhao, Z.-F., Gao, S., Wu, F.Y., 2006a. Zircon U–Pb age and Hf-O isotope evidence for Paleoproterozoic metamorphic event in south China. Precambrian Res. 151, 265–288.

Zhang, S.-B., Zheng, Y.-F., Wu, Y.-B., Zhao, Z.-F., Gao, S., Wu, F.Y., 2006b. Zircon isotope evidence for >3.5 Ga continental crust in the Yangtze craton of China. Precambrian Res. 146, 16–34.

Zhang, Z.M., Schertl, H.P., Wang, J.L., Shen, K., Liou, J.G., 2009. Source of coesite inclusions within inherited magmatic zircon from Sulu UHP rocks, eastern China, and their bearing for fluid-rock interaction and SHRIMP dating. J. Metamorph. Geol. 27, 317–333.

Zhang, Y.F., Wu, Y., Wang, C., Jin, Z.M., Schertl, H.P., 2014. Experimental constraints on the genesis of jadeite quartzite from Shuanghe, Dabie mountain ultra-high pressure metamorphic terrane. Sci. China Earth Sci. 57, 104–116.

Zheng, Y.-F., 2008. A perspective view on ultrahigh-pressure metamorphism and continental collision in the Dabie-Sulu orogenic belt. Chin. Sci. Bull. 53, 3081–3104.

Zheng, Y.F., 2009. Fluid regime in continental subduction zones: petrological insights from ultrahigh-pressure metamorphic rocks. J. Geol. Soc. 166, 763–782.

Zheng, Y.-F., 2012. Metamorphic chemical geodynamics in continental subduction zones. Chem. Geol. 328, 5–48.

Zheng, Y.-F., Fu, B., Li, Y.-L., Xiao, Y.L., Li, S.G., 1998. Oxygen and hydrogen isotope geochemistry of ultrahigh-pressure eclogites from the Dabie mountains and Sulu terrane. Earth Planet. Sci. Lett. 155, 113–129.

Zheng, Y.-F., Fu, B., Gong, B., Li, L., 2003. Stable isotope geochemistry of ultrahigh pressure metamorphic rocks from the Dabie-Sulu orogen in China: implications for geodynamics and fluid regime. Earth-Sci. Rev. 62, 105–161.

Zheng, Y.-F., Wu, Y.-B., Chen, F.-K., Gong, B., Li, L., Zhao, Z.-F., 2004. Zircon U–Pb and oxygen isotope evidence for a large-scale ^{18}O depletion event in igneous rocks during the Neoproterozoic. Geochim. Cosmochim. Acta 68, 4145–4165.

Zheng, Y.-F., Wu, Y.-B., Zhao, Z.-F., Zhang, S.-B., Xu, P., Wu, F.-Y., 2005. Metamorphic effect on zircon Lu–Hf and U–Pb isotope systems in ultrahigh-pressure eclogite-facies metagranite and metabasite. Earth Planet. Sci. Lett. 240, 378–400.

Zheng, Y.-F., Zhao, Z.-F., Wu, Y.-B., Zhang, S.-B., Liu, X.M., Wu, F.-Y., 2006. Zircon U–Pb age, Hf and O isotope constraints on protolith origin of ultrahigh-pressure eclogite and gneiss in the Dabie orogen. Chem. Geol. 231, 135–158.

Zheng, Y.-F., Gao, T.-S., Wu, Y.-B., Gong, B., Liu, X.-M., 2007. Fluid flow during exhumation of deeply subducted continental crust: Zircon U–Pb age and O-isotope studies of a quartz vein within ultrahigh-pressure eclogite. J. Metamorph. Geol. 25, 267–283.

Zheng, Y.F., Chen, R.X., Zhao, Z.F., 2009. Chemical geodynamics of continental subduction-zone metamorphism: insights from studies of the Chinese continental scientific drilling (CCSD) core samples. Tectonophysics 475, 327–358.

Zheng, Y.-F., Xia, Q.-X., Chen, R.-X., Gao, X.-Y., 2011. Partial melting, fluid supercriticality and element mobility in ultrahigh-pressure metamorphic rocks during continental collision. Earth Sci. Rev. 107, 342–374.